IEEE Access
Multidisciplinary | Rapid Review | Open Access Journal

Received March 18, 2019, accepted March 28, 2019, date of publication April 9, 2019, date of current version April 22, 2019.

Digital Object Identifier 10.1109/ACCESS.2019.2909987

Generalized Signal-Space Alignment Based Physical-Layer Network Coding for Distributed MIMO Systems

HAI CHENG[1], XIAOJUN YUAN[1], (Senior Member, IEEE), AND TAO YANG[2], (Member, IEEE)

[1]National Key Laboratory of Science and Technology on Communication, Center for Intelligent Networking and Communications, University of Electronic Science and Technology of China, Chengdu 611731, China

[2]Beijing University of Aeronautics and Astronautics, Beijing 100083, China

Corresponding authors: Xiaojun Yuan (xjyuan@uestc.edu.cn) and Tao Yang (tyang@buaa.edu.cn)

The work of X. Yuan was supported in part by the China Recruitment Program of Global Young Experts, and in part by the Key Areas R&D Plan of Guangdong China under Grant 2018B010114001. The work of T. Yang was supported by the Beihang ''Zhuoyue'' Program and the ARC Discovery Early Career Researcher Award under Project DE150100636.

ABSTRACT We study an uplink distributed multiple-input-multiple-output (D-MIMO) system, where multiple users are served by multiple base stations (BSs) connected to a common central unit (CU). We propose a generalized signal-space alignment (SSA)-based physical-layer network coding (PNC) scheme, termed G-SSA-PNC. In G-SSA-PNC, the multi-antenna users encode their messages by using nested lattice coding, linearly precode the nested lattice codewords for SSA, and then broadcast to the multi-antenna BSs. The BSs linearly post-process the received signals to extract signals at certain aligned directions. PNC decoding is applied to those extracted signals to generate network-coded message combinations, and the decoded message combinations are then forwarded to the CU for user messages decoding. Compared with the original SSA-PNC scheme, our scheme is different in the following three aspects. *First*, the G-SSA-PNC employs an individual shaping lattice for nested lattice coding at each source, as in contrast to the use of a common shaping lattice in original SSA-PNC. *Second*, we derive the feasibility condition of PNC decoding under the new nested lattice coding scheme and show that the SSA precoding and the nested lattice coding needs to be jointly designed to meet the feasibility condition. *Third*, we formulate a sum rate maximization problem and propose a suboptimal solution to the problem. The numerical results demonstrate the superiority of the G-SSA-PNC in performance over the benchmark schemes, including original SSA-PNC, compress-and-forward, and interference alignment.

INDEX TERMS Distributed MIMO systems, interference alignment, nested lattice coding, physical-layer network coding, signal-space alignment.

I. INTRODUCTION

To accommodate exponentially increasing demands for data services, advanced technologies, such as multiple-input multiple-output (MIMO) and hyper-dense cellular systems, are employed in LTE-advanced and fifth-generation (5G) cellular networks. The performance of these networks is largely limited by inter-cell interference. Traditional cellular systems employ orthogonalization methods (e.g., the frequency-reuse and the time-reuse) to mitigate the interference, or utilize sophisticated signal processing methods to suppress interference. Cloud radio access network (Cloud-RAN) [1] is a new network architecture which can harness interference more efficiently. The main idea is that, by allowing cooperation and joint signal processing across different cells, the inter-cell interference can be used to enhance the throughput. A distributed MIMO (D-MIMO) system can be regarded as a MIMO Cloud-RAN, where multi-antenna users communicates to a central unit (CU) with the help of multi-antenna base stations (BSs). There is no direct link between the users and the CU. The BSs are connected to the CU through independent backhaul links with individual maximum throughput constraints. Note that the D-MIMO system model applies to both wired and wireless backhaul transmissions.

An important issue in D-MIMO systems is how to efficiently utilize interference in joint signal processing. In the past several years, many progresses have been made towards the issue [2]–[15]. One approach is to treat interference as noise and to obtain an achievable rate from an

The associate editor coordinating the review of this manuscript and approving it for publication was Liang Yang.

information theoretical perspective [2]–[4]. Compress-and-forward (CoF) relaying is applied to analyze the achievable rate of uplink D-MIMO systems. It is shown in [2] that joint decompression and decoding at CU is advantageous over separated operations. In [3], [4], the authors proposed a virtual multiple access channel (VMAC) scheme involving Wyner-Ziv coding in BSs and successive decoding of compressed codewords and user messages. The network performance is improved by maximizing the achievable sum rate over the beamforming matrices at users and the quantization noises at BSs.

A second approach is to orthogonalize the desired signals and the interference in the received signal-space through interference alignment (IA). For example, the IA technique can improve the degrees of freedom (DoF) of a K user time-varying interference channel from 1 to $\frac{K}{2}$ [6]. After its advent, IA has been extensively applied to analyze the performance limits of various MIMO interference channels [7]–[10]. In [7], the feasibility of interference alignment in signal space is related to the solvability of a polynomial system. In [9], an iterative algorithm is proposed to find the maximum sum-rate in MIMO interference channels.

A third approach is to regard the interference as useful signals. For example, compute-and-forward strategy [11], as an implementation of physical-layer network coding (PNC), harnesses interference through lattice codes. In the original compute-and-forward scheme [11], single-antenna users and relays are considered. With nested lattice coding, each relay computes a linear combination of user messages from the received signal and forwards the messages combinations to CU.

More recently, the work [12] proposed a physical-layer network coding (PNC) scheme for D-MIMO systems employing signal-space alignment (SSA). We refer to the approach in [12] as SSA-PNC. In SSA-PNC, with carefully designed network-coding and beamforming matrices, the transmitted signals are aligned at BSs according to predetermined patterns, and linear message combinations are computed at each BS from the aligned signals. It is demonstrated that the achievable DoF of the SSA-PNC scheme is considerably higher than those schemes that directly utilize IA.

However, there are several important open issues regarding the SSA-PNC scheme. First, SSA-PNC assumed a common shaping lattice in the construction of nested lattice codes at the users. Second, in SSA-PNC, the received power ratios of the spatial streams aligned in a spatial direction directly determine the corresponding network coded messages. Third, the linear precoding matrices for SSA and the network coding coefficients for PNC are not appropriately optimized for performance improvement.

In this paper, we propose a generalized SSA-PNC (G-SSA-PNC) scheme for the D-MIMO system to address the above three open issues. In the proposed scheme, the multi-antenna users encode their messages by using nested lattice coding, linearly precode the nested lattice codewords for SSA, and then broadcast to the multi-antenna BSs. The BSs linearly post-process the received signals from the users to extract signals at certain aligned directions. PNC decoding is applied to those extracted signals. Finally, the decoded messages are forwarded through the backhaul to the CU for user message recovery.

We summarize the novelty and contribution of our work as follows. G-SSA-PNC allows the use of different shaping lattices at different sources, as well as different precoding and channel gains for different spatial streams at the BSs. This gives more freedom for the design of nested lattice coding to match the channel conditions. The challenge is how to preserve the nested lattice structure at the BSs, especially when each BS computes multiple message combinations. As one of our main contributions, we show that certain feasibility conditions on the joint design of SSA precoding and nested lattice coding need to be met, so as to ensure the nested lattice structure at the BSs.[1] With the derived feasibility conditions, we establish an achievable rate region and formulate a sum-rate optimization problem for the G-SSA-PNC scheme. The problem is non-convex and we propose an approximate solution to the problem. We show by simulations the superiority of the G-SSA-PNC over several baseline schemes, including interference alignment, compress-and-forward, generalized compute-compress-and-forward (GCCF) [16], and decode-and-forward.

The paper is organized as follows. The system model is presented in Section II. The optimized SSA-PNC scheme is discussed in Section III. The feasibility of the proposed scheme is investigated in Section IV. The sum-rate maximization problem is formulated and the corresponding algorithm is presented in V. The numerical results and the conclusions are given in Section VI and VII, respectively. Throughout this paper, lowercase boldface letters (e.g., $\boldsymbol{b}$) are used to denote column vectors, and uppercase boldface letters (e.g., $\boldsymbol{H}$) are used to denote matrices. Frequently used notations are summarized in Table 1.

II. SYSTEM MODEL

Following [12], we consider a D-MIMO network with K users and J base stations (BSs), as illustrated in Fig. 1. Each user is equipped with N antennas and each BS is equipped with M antennas. All the BSs connect to a common central unit (CU) via an error-free backhaul link with a limited capacity. We assume that users are geographically separated and so are the BSs.

The D-MIMO network consists of two layers, namely, the air-interface layer and the backhaul layer. In the air-interface layer, the K users transmit individual messages to the J BSs. In the *backhaul* layer, each BS processes its received signal and forwards the processed signal to the CU

[1] In original SSA-PNC, all the sources employ a common shaping lattice, and in each aligned spatial direction the combined precoding and channel gains of the spatial streams are forced to have integer ratios. Such a treatment naturally preserves the nested lattice structure at the BSs, but at the same time causes significant performance loss, as revealed by the simulation results presented later.

TABLE 1. Frequently used notations.

Notation	Definition
$\boldsymbol{b}_k$	The message of the k-th user
$\boldsymbol{b}_{k,l}$	The l-th data stream of user k
$\mathcal{I}_K$	The index set $\{1, 2, \cdots, K\}$
$\boldsymbol{c}_{k,l}$	The l-th spatial stream of user k
$\mathbb{Z}^q$	The additive group with elements $\{0, 1, \cdots, q-1\}$
$\boldsymbol{P}_k$	The precoding matrix of user k
$\boldsymbol{p}_{k,l}$	The l-th column of $\boldsymbol{P}_k$
$\boldsymbol{X}_k$	The channel input signal of user k
$\boldsymbol{Y}_j$	The received signal of BS j
$\boldsymbol{H}_{j,k}$	The channel coefficient matrix from user k to BS j
Λ	A lattice over $\mathbb{R}^n$
σ_Λ	The square root of the second moment of Λ
$\mathcal{L}$	A nested lattice chain with $2L$ lattices
$\boldsymbol{g}_{j,m,k}$	An integer vector
$g_{j,m,k,l}$	The l-th element of $\boldsymbol{g}_{j,m,k}$
$\widetilde{\boldsymbol{G}}$	The generator matrix of an alignment pattern
$\boldsymbol{B}_k$	The zero-padded message sequence of user k in matrix form
$\boldsymbol{u}_{j,i}$	The i-th network-coded message sequence of BS j
$\boldsymbol{G}$	The network-coding matrix
$\beta_{j,m,k,l}$	A non-zero real coefficient
$\boldsymbol{F}_j$	The shaping matrix of BS j
$\boldsymbol{T}_j$	The shaped signal of BS j

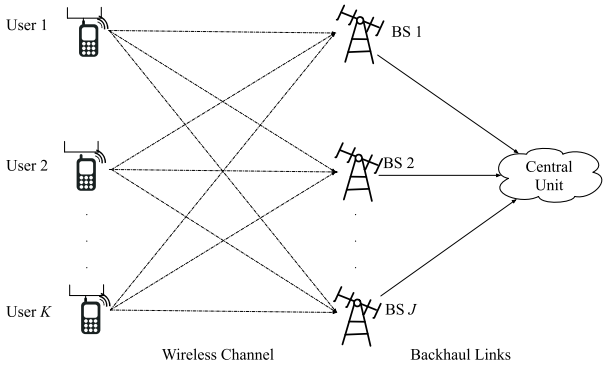

FIGURE 1. System model.

via the backhaul link. After receiving signals from the J BSs, the CU manages to recover all the messages from the K users.

1) AIR-INTERFACE LAYER

Denote by $\boldsymbol{b}_k \in \mathbb{F}_q^{s_k \times 1}$ the message of user k, where s_k is an integer, q is a prime number, and $\mathbb{F}_q$ is a finite field with q elements. User k encodes $\boldsymbol{b}_k$ into a real N-by-n space-time signal matrix

$$\boldsymbol{X}_k = \phi_k(\boldsymbol{b}_k), \quad k \in \mathcal{I}_K \triangleq \{1, 2, \cdots, K\}, \tag{1}$$

where n is the number of channel use. The function $\phi_k(\cdot)$ represents the encoding at user k, which is elaborated in Section III-A.1. Then, the entropy rate of user k is $R_k = \frac{s_k}{n} \log_2 q$ bits per channel use. Consider a block fading channel in the air-interface layer, i.e. the channel coefficients remain constant over a block of n channel uses and vary from block to block. In a block, BS j observes a channel output matrix

$$\boldsymbol{Y}_j = \sum_{k=1}^{K} \boldsymbol{H}_{j,k} \boldsymbol{X}_k + \boldsymbol{Z}_j, \quad j \in \mathcal{I}_J. \tag{2}$$

where $\boldsymbol{H}_{j,k} \in \mathbb{R}^{M \times N}$ is the flat-fading channel coefficient matrix from user k to BS j, and $\boldsymbol{Z}_j \in \mathbb{R}^{M \times n}$ is the additive white Gaussian noise (AWGN) matrix with independent and identically distributed (i.i.d.) elements of zero mean and σ_z^2 variance. The power constraint of each user k is given by

$$\frac{1}{n} \mathbb{E}\left(\mathrm{tr}(\boldsymbol{X}_k^{\mathrm{T}} \boldsymbol{X}_k)\right) \leq P_k, \quad k \in \mathcal{I}_K. \tag{3}$$

2) BACKHAUL LAYER

After receiving $\boldsymbol{Y}_j$, BS j decodes $\hat{\boldsymbol{U}}_j$ from $\boldsymbol{Y}_j$, where $\hat{\boldsymbol{U}}_j$ is an estimate of $\boldsymbol{U}_j$ that is a certain deterministic function of the source messages.[2] Then, BS j forwards $\hat{\boldsymbol{U}}_j$ to the CU through its backhaul link. In this paper, we consider a total backhaul rate constraint as in [3], [12]. Lossless distributed source coding [17] can be applied to $\{\hat{\boldsymbol{U}}_j\}$ at BSs. From the Slepian-Wolf coding [18] and GCCF, the transmission over backhaul links is error-free if the following constraint is met:

$$\frac{1}{n} H(\hat{\boldsymbol{U}}_1, \hat{\boldsymbol{U}}_2, \cdots, \hat{\boldsymbol{U}}_J) \leq C_{\mathrm{BH}} \tag{4}$$

where $H(\cdot)$ denotes the entropy function, and C_{BH} is the total capacity of all the J backhaul links.

After receiving $\hat{\boldsymbol{U}}_j, j \in \mathcal{I}_J$, the CU needs to recover all K users' messages $\{\hat{\boldsymbol{b}}_k, k \in \mathcal{I}_K\}$. The decoded user messages are represented by

$$(\hat{\boldsymbol{b}}_1, \hat{\boldsymbol{b}}_2, \cdots, \hat{\boldsymbol{b}}_K) = \Theta(\hat{\boldsymbol{U}}_1, \hat{\boldsymbol{U}}_2, \cdots, \hat{\boldsymbol{U}}_J) \tag{5}$$

where $\Theta(\cdot)$ denotes the decoding operation. The decoding is successful if $\hat{\boldsymbol{b}}_k = \boldsymbol{b}_k$ for all $k \in \mathcal{I}_K$. A rate tuple $(R_1, R_2, \cdots, R_K)$ is said to be *achievable* if the decoding error probability satisfies

$$Pr\left\{(\hat{\boldsymbol{b}}_1, \hat{\boldsymbol{b}}_2, \cdots, \hat{\boldsymbol{b}}_K) \neq (\boldsymbol{b}_1, \boldsymbol{b}_2, \cdots, \boldsymbol{b}_K)\right\} < \epsilon \tag{6}$$

for any $\epsilon > 0$ as the block length $n \to \infty$. Our goal is to design a transceiver scheme for the D-MIMO system presented above with a high achievable sum rate.

Full channel state information (CSI) is assumed in this paper. That is, every node in the network knows all the channel matrices in the network. This is, however, difficult to realize in practical scenarios. In practice, our proposed G-SSA-PNC scheme can be realized as follows. Each BS j

[2] We defer the specification of the size of $\boldsymbol{U}_j$ to Section III-C.

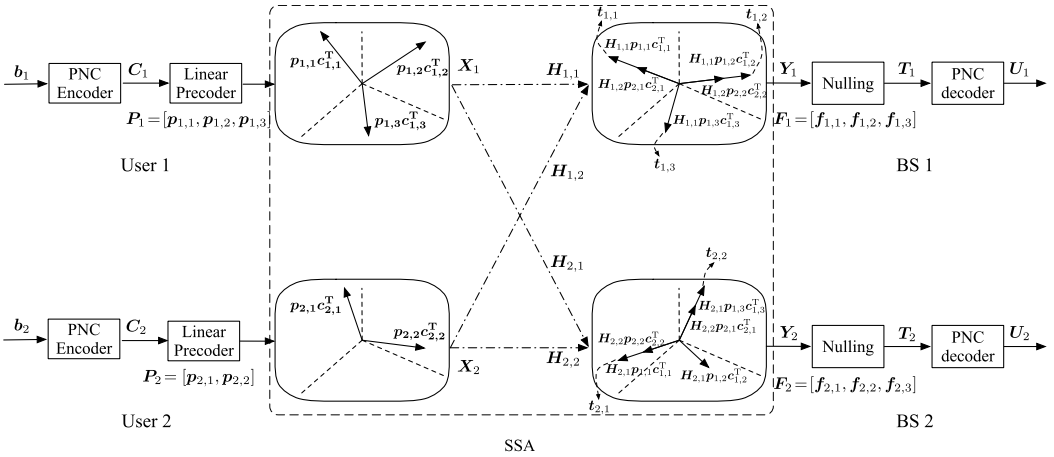

FIGURE 2. An example of the operations at users and BSs in the SSA-PNC approach.

estimates its channels and then forward the estimated channels to CU. With full CSI, CU is able to compute the construction of nested lattice codes, the linear precoding matrices at the users, and the post-processing matrices at BSs, etc. Then, CU sends the computed information back to BSs and users through the backhaul links and the wireless links between BSs and users.

III. GENERALIZED SSA-PNC SCHEME

In this section, we describe a novel SSA-PNC approach, as illustrated in Fig. 2. Note that the scheme in Fig. 2 is similar to the SSA-PNC scheme in [12]. The difference of our approach will be elaborated in Remarks 1, 3, 4, and Subsection III-F.

A. ENCODING AT USERS

1) NESTED LATTICE CODING

The encoding operation is carried out as follows. The message $\boldsymbol{b}_k \in \mathbb{F}_q^{s_k \times 1}$ of user k is firstly segmented into L_k parts as $\boldsymbol{b}_k = [\boldsymbol{b}_{k,1}^{\mathrm{T}}, \boldsymbol{b}_{k,2}^{\mathrm{T}}, \cdots, \boldsymbol{b}_{k,L_k}^{\mathrm{T}}]^{\mathrm{T}}$, where $\boldsymbol{b}_{k,l}$ is the l-th *data stream* of user k, and L_k is the total number of data streams of user k. Denote by $s_{k,l}$ the length of $\boldsymbol{b}_{k,l}$ and $R_{k,l}$ the rate of $\boldsymbol{b}_{k,l}$. Clearly, $\sum_{l=1}^{L_i} s_{k,l} = s_k$. The total number of data streams of K users is given by $L = \sum_{k=1}^{K} L_k$.

Nested lattice coding [19] is applied to encode data stream $\boldsymbol{b}_{k,l}$. To this end, we construct a nested lattice chain with $2L$ lattices using Construction A [11]

$$\mathcal{L} \triangleq \{\{\Lambda_l\}_{l=1}^{2L} | \Lambda_1 \subseteq \Lambda_2 \subseteq \cdots \subseteq \Lambda_{2L}\} \tag{7}$$

We divide all lattices in the nested lattice chain $\mathcal{L}$ as L lattice pairs $(\Lambda_{s,k,l}, \Lambda_{c,k,l})$ for $k \in \mathcal{I}_K$ and $l \in \mathcal{I}_{L_k}$. The corresponding nested lattice codebook for $(\Lambda_{s,k,l}, \Lambda_{c,k,l})$ is given by $\mathcal{C}_{k,l} = \Lambda_{c,k,l} \bmod \Lambda_{s,k,l}$. In encoding, each data stream $\boldsymbol{b}_{k,l}$ is mapped to a *spatial stream* $\boldsymbol{c}_{k,l} \in \mathbb{R}^{n \times 1}$ using the lattice codebook $\mathcal{C}_{k,l}$. The normalized codeword matrix of user k is defined as

$$\boldsymbol{C}_k = \left[\frac{\boldsymbol{c}_{k,1}}{\sigma_{\mathrm{s},k,1}}, \frac{\boldsymbol{c}_{k,2}}{\sigma_{\mathrm{s},k,2}}, \cdots, \frac{\boldsymbol{c}_{k,L_k}}{\sigma_{\mathrm{s},k,L_k}}\right]^{\mathrm{T}} \in \mathbb{R}^{L_k \times n} \tag{8}$$

where $\sigma_{\mathrm{s},k,l}^2$ is the second moment of $\Lambda_{\mathrm{s},k,l}$.

Remark 1: The proposed scheme employs an individual shaping lattice $\Lambda_{s,k,l}$ for each $\mathcal{C}_{k,l}$, as in contrast to the use of a common shaping lattice in SSA-PNC [12]. This generalization gives more freedom for the design of nested lattice coding to match the channel conditions. At the same time, this generalization introduces additional constraints for the joint design of SSA and nested lattices, as will be elaborated in Section IV.

Remark 2: In practice, non-binary linear codes such as irregular non-binary repeat accumulate codes [13] with low complexity iterative belief propagation decoding algorithms can be used to support physical-layer network coding. However, these schemes with practical codes are difficult to analyze. Here we use nested lattice codes to derive an achievable rate region of the generalized SSA-PNC scheme.

2) DISTRIBUTED LINEAR PRECODING

After obtaining $\boldsymbol{C}_k$, each user performs linear precoding to generate the channel input signal

$$\boldsymbol{X}_k = \boldsymbol{P}_k \boldsymbol{C}_k, \quad k \in \mathcal{I}_K \tag{9}$$

where $\boldsymbol{P}_k \in \mathbb{R}^{N \times L_k}$ is the linear precoding matrix of user k. Then, the l-th column of $\boldsymbol{P}_k$, denoted by $\boldsymbol{p}_{k,l}$, specifies the *signal space* of the l-th spatial stream of user k. Since each user has N antennas, the number of independent spatial streams for each user is at most N, i.e. $L_k \leq N, k \in \mathcal{I}_K$. Note that $\{\boldsymbol{c}_{k,l}\}$ are independent spatial streams and so

$$\frac{1}{n}\mathbb{E}\left(\boldsymbol{C}_k \boldsymbol{C}_k^{\mathrm{T}}\right) = \boldsymbol{I}. \tag{10}$$

Then, the power constraint in (3) can be rewritten as

$$\mathrm{tr}(\boldsymbol{P}_k \boldsymbol{P}_k^{\mathrm{T}}) \leq P_k, \quad k \in \mathcal{I}_K. \tag{11}$$

B. SIGNAL-SPACE ALIGNMENT

In this section, we propose to align the received spatial streams at BSs in a required manner. By the projection of channel matrix, the signal-space of spatial stream $\boldsymbol{c}_{k,l}$ at BS j is given by $\boldsymbol{H}_{j,k}\boldsymbol{p}_{k,l}$. Thus, to align $\boldsymbol{c}_{k_1,l_1}$ with $\boldsymbol{c}_{k_2,l_2}$ at BS j, it is required to design $\boldsymbol{p}_{k_1,l_1}$ and $\boldsymbol{p}_{k_2,l_2}$ satisfying

$$\boldsymbol{H}_{j,k_1}\boldsymbol{p}_{k_1,l_1} \parallel \boldsymbol{H}_{j,k_2}\boldsymbol{p}_{k_2,l_2} \tag{12}$$

where "$\parallel$" stands for parallelism. Since each BS has M antennas, all L spatial streams need to be aligned in the signal-spaces with dimension M.

To represent the alignment pattern, we define an integer vector $\boldsymbol{g}_{j,m,k} \in \mathbb{Z}_q^{L_k}$. Denote the support set for $\boldsymbol{g}_{j,m,k}$ as

$$\mathcal{S}(\boldsymbol{g}_{j,m,k}) \triangleq \{l : g_{j,m,k,l} \neq 0\}, \tag{13}$$

where $g_{j,m,k,l}$ is the l-th element in $\boldsymbol{g}_{j,m,k}$. For any $l_1 \in \mathcal{S}(\boldsymbol{g}_{j,m,k_1})$, $l_2 \in \mathcal{S}(\boldsymbol{g}_{j,m,k_2})$, our objective is to align $\boldsymbol{c}_{k_1,l_1}$ and $\boldsymbol{c}_{k_2,l_2}$ in the m-th aligned direction of BS j, i.e. to satisfy (12). Thus, the alignment pattern is determined by given $\{\boldsymbol{g}_{j,m,k}, j \in \mathcal{I}_J, m \in \mathcal{I}_M, k \in \mathcal{I}_K\}$. The signal-space alignment criterion is formally presented below.

Criterion 1: For BS j, the signal-spaces of its received spatial streams are aligned according to $\{\boldsymbol{g}_{j,m,k}, m \in \mathcal{I}_M, k \in \mathcal{I}_K\}$, *i.e., for any* $k_1, k_2 \in \mathcal{I}_K$,

$$\beta_{j,m,k_1,l_1}\boldsymbol{H}_{j,k_1}\boldsymbol{p}_{k_1,l_1} = \beta_{j,m,k_2,l_2}\boldsymbol{H}_{j,k_2}\boldsymbol{p}_{k_2,l_2}, \quad l_1 \in \mathcal{S}(\boldsymbol{g}_{j,m,k_1}), l_2 \in \mathcal{S}(\boldsymbol{g}_{j,m,k_2}), \tag{14}$$

where β_{j,m,k_1,l_1} *and* β_{j,m,k_2,l_2} *are non-zero real coefficients.*

Remark 3: Note that (14) *reduces to the original SSA-PNC [12] by letting* $\beta_{j,m,k_1,l_1} = g_{j,m,k_1,l_1}$ *and* $\beta_{j,m,k_2,l_2} = g_{j,m,k_2,l_2}$. *Here, we allow* $\{\beta_{j,m,k,l}\}$ *to be arbitrary non-zero real numbers. That is, the power ratio of the received spatial stream at one aligned direction,* $|\frac{\boldsymbol{H}_{j,k_1}\boldsymbol{p}_{k_1,l_1}}{\boldsymbol{H}_{j,k_2}\boldsymbol{p}_{k_2,l_2}}|$, *is decoupled from the coefficient ratio* $|\frac{g_{j,m,k_1,l_1}}{g_{j,m,k_2,l_2}}|$ *in original SSA-PNC. This decoupling gives more freedom to the system design as well as the system performance optimization.*

Example 1: An example is given in Fig. 2 to illustrate SSA precoding. In the example, we set $K = J = 2, N = M = 3, L_1 = 3,$ and $L_2 = 2$. All integer vectors are given as

$$\begin{aligned}
&\boldsymbol{g}_{1,1,1}^{\mathrm{T}} = [1,0,0], \quad \boldsymbol{g}_{1,2,1}^{\mathrm{T}} = [0,1,0], \quad \boldsymbol{g}_{1,3,1}^{\mathrm{T}} = [0,0,1]\\
&\boldsymbol{g}_{1,1,2}^{\mathrm{T}} = [1,0], \quad \boldsymbol{g}_{1,2,2}^{\mathrm{T}} = [0,1], \quad \boldsymbol{g}_{1,3,2}^{\mathrm{T}} = [0,0]\\
&\boldsymbol{g}_{2,1,1}^{\mathrm{T}} = [0,0,1], \quad \boldsymbol{g}_{2,2,1}^{\mathrm{T}} = [1,0,0], \quad \boldsymbol{g}_{2,3,1}^{\mathrm{T}} = [0,1,0]\\
&\boldsymbol{g}_{2,1,2}^{\mathrm{T}} = [1,0], \quad \boldsymbol{g}_{2,2,2}^{\mathrm{T}} = [0,1], \quad \boldsymbol{g}_{2,3,2}^{\mathrm{T}} = [0,0].
\end{aligned}$$

Since $\mathcal{S}(\boldsymbol{g}_{1,1,1}) = 1, \mathcal{S}(\boldsymbol{g}_{1,1,2}) = 1$, we need to align spatial stream $\boldsymbol{c}_{1,1}$ and $\boldsymbol{c}_{2,1}$ in the 1st aligned direction of BS 1. Then, $\boldsymbol{p}_{1,1}$ and $\boldsymbol{p}_{2,1}$ satisfy $\beta_{1,1,1,1}\boldsymbol{H}_{1,1}\boldsymbol{p}_{1,1} = \beta_{1,1,2,1}\boldsymbol{H}_{1,2}\boldsymbol{p}_{2,1}$. The other constraints can be obtained in a similar way. □

To represent the alignment pattern conveniently, we denote

$$\boldsymbol{g}_{j,m} \triangleq [\boldsymbol{g}_{j,m,1}^{\mathrm{T}}, \boldsymbol{g}_{j,m,2}^{\mathrm{T}}, \cdots, \boldsymbol{g}_{j,m,K}^{\mathrm{T}}]^{\mathrm{T}}, \tag{15}$$

$$\tilde{\boldsymbol{G}}_j \triangleq [\boldsymbol{g}_{j,1}, \boldsymbol{g}_{j,2}, \cdots, \boldsymbol{g}_{j,M}]. \tag{16}$$

Thus, $\tilde{\boldsymbol{G}}_j \in \mathbb{Z}^{L\times M}$ specifies the alignment pattern at BS j. Since every spatial stream can be and only be aligned in one direction at each BS, the number of non-zero elements of each row in $\tilde{\boldsymbol{G}}_j$ is 1. The *generator matrix* is defined by

$$\tilde{\boldsymbol{G}} \triangleq [\tilde{\boldsymbol{G}}_1, \tilde{\boldsymbol{G}}_2, \cdots, \tilde{\boldsymbol{G}}_J]. \tag{17}$$

The generator matrix consisting the integer vectors in Example 1 is given by

$$\tilde{\boldsymbol{G}} = \begin{bmatrix} 1 & 0 & 0 & 0 & 1 & 0 \\ 0 & 1 & 0 & 0 & 0 & 1 \\ 0 & 0 & 1 & 1 & 0 & 0 \\ 1 & 0 & 0 & 1 & 0 & 0 \\ 0 & 1 & 0 & 0 & 1 & 0 \end{bmatrix} \tag{18}$$

Note that $\tilde{\boldsymbol{G}}$ determines the alignment pattern of the D-MIMO system. Also note that the existence of $\{\boldsymbol{P}_k\}$ satisfying (14) for a given generator matrix $\tilde{\boldsymbol{G}}$ is not always guaranteed. The feasibility condition of signal-space alignment will be discussed in Section IV-A.

C. BS PROCESSING

By substituting (9) into (2), we obtain the received signal at BS j:

$$\boldsymbol{Y}_j = \sum_{k=1}^{K}\sum_{l=1}^{L_k} \boldsymbol{H}_{j,k}\boldsymbol{p}_{k,l}\frac{\boldsymbol{c}_{k,l}^{\mathrm{T}}}{\sigma_{\mathrm{s},k,l}} + \boldsymbol{Z}_j, j \in \mathcal{I}_J. \tag{19}$$

In the above, $\boldsymbol{Y}_j$ is a summation of L received spatial streams. For BS j, it is required to decode linear combinations of data streams based on $\boldsymbol{Y}_j$. In the following, we first introduce some concepts about network-coding and then present the detailed operations at BSs, including nulling and network-coded decoding.

1) NETWORK-CODED MESSAGES

Following [16], we zero-pad $\boldsymbol{b}_{k,l}$ with length $s_{k,l}$ to $\tilde{\boldsymbol{b}}_{k,l}$ with common length $s_{\max} \triangleq \max_{k,l} s_{k,l}$. Then, we rewrite the message of user k as

$$\boldsymbol{B}_k = [\tilde{\boldsymbol{b}}_{k,1}, \tilde{\boldsymbol{b}}_{k,2}, \cdots, \tilde{\boldsymbol{b}}_{k,L_k}] \in \mathbb{F}_q^{s_{\max}\times L_k}. \tag{20}$$

Then, the messages of all K users can be rewritten as

$$\boldsymbol{B} = [\boldsymbol{B}_1, \boldsymbol{B}_2, \cdots, \boldsymbol{B}_K] \in \mathbb{F}_q^{s_{\max}\times L}. \tag{21}$$

A *network-coded message* is a linear combination of all users' messages and is represented by

$$\boldsymbol{u} = \boldsymbol{B}\varphi(\boldsymbol{g}) \in \mathbb{F}_q^{s_{\max}} \tag{22}$$

where $\boldsymbol{g} \in \mathbb{Z}_q^L$ is referred to as a network-coded *coefficient vector*, and $\varphi(\cdot)$ maps $\mathbb{Z}_q$ into $\mathbb{F}_q$. Note that for a vector or matrix input, $\varphi(\cdot)$ is applied in an element-wise manner.

BS j attempts to generate L_j' network-coded message $\boldsymbol{u}_{j,1}, \boldsymbol{u}_{j,2}, \cdots, \boldsymbol{u}_{j,L_j'}$ from $\boldsymbol{Y}_j$. We assume $L_j' \leq M$ by noting that the dimension of the signal space of receiver j is M. We choose the network-coded coefficient vectors of $\boldsymbol{u}_{j,i}$ as $\boldsymbol{g}_{j,i}$ for $i = 1, 2, \cdots, L_j'$.

Rewrite the network-coded messages and the corresponding coefficient vectors in a matrix form:

$$\boldsymbol{U}_j = [\boldsymbol{u}_{j,1}, \boldsymbol{u}_{j,2}, \cdots, \boldsymbol{u}_{j,L_j'}] \in \mathbb{F}_q^{s_{\max} \times L_j'} \tag{23}$$

$$\boldsymbol{G}_j = [\boldsymbol{g}_{j,1}, \boldsymbol{g}_{j,2}, \cdots, \boldsymbol{g}_{j,L_j'}] \in \mathbb{Z}_q^{L \times L_j'}. \tag{24}$$

Then, we have

$$\boldsymbol{U}_j = \boldsymbol{B}\varphi(\boldsymbol{G}_j). \tag{25}$$

Note that $\boldsymbol{G}_j$ consists of the first L_j' columns of $\tilde{\boldsymbol{G}}_j$.

The total number of network-coded message sequences of all BSs is given by $L' = \sum_{j=1}^{J} L_j'$. Then, the network-coded message all J BSs are given by

$$\boldsymbol{U} = [\boldsymbol{U}_1, \boldsymbol{U}_2, \cdots, \boldsymbol{U}_J] = \boldsymbol{B}\varphi(\boldsymbol{G}) \tag{26}$$

where $\boldsymbol{G} \triangleq [\boldsymbol{G}_1, \boldsymbol{G}_2, \cdots, \boldsymbol{G}_J] \in \mathbb{Z}_q^{L \times L'}$ is referred to as the *network-coding matrix*. As all user messages need to be recovered from $\boldsymbol{U}$, it is required that the rank of $\varphi(\boldsymbol{G})$ is no less than L.

Criterion 2: The rank of $\varphi(\boldsymbol{G})$ is no less than L.

Criterion 2 implies $L' \geq L$, where L' is the total number of network-coded messages decoded at the J BSs. In this paper, we always assume $L' = L$ to reduce the consumption of the backhaul capacity.

2) NULLING AT BSS

In the receiver shaping step, BS j processes the received signal $\boldsymbol{Y}_j$ by performing a linear transformation to $\boldsymbol{Y}_j$

$$\boldsymbol{T}_j = \boldsymbol{F}_j \boldsymbol{Y}_j, \quad j \in \mathcal{I}_J \tag{27}$$

where $\boldsymbol{F}_j \in \mathbb{R}^{L_j' \times M}$ and $\boldsymbol{T}_j \in \mathbb{R}^{L_j' \times n}$. Denote by $\boldsymbol{f}_{j,i}^{\mathrm{T}}$ and $\boldsymbol{t}_{j,i}^{\mathrm{T}}$ the i-th row of $\boldsymbol{F}_j$ and $\boldsymbol{T}_j$, respectively. With carefully chosen $\boldsymbol{f}_{j,i}$, $\boldsymbol{t}_{j,i}$ only consists of the spatial streams in the i-th aligned direction of BS j (specified by indicator vector $\boldsymbol{g}_{j,i}$). Specifically, we introduce the following nulling criteria:

Criterion 3: For any given $j \in \mathcal{I}_J$, $i \in \mathcal{I}_{L_j'}$, the unit vector $\boldsymbol{f}_{j,i}$ (with $\|\boldsymbol{f}_{j,i}\| = 1$) satisfies

$$\boldsymbol{f}_{j,i}^{\mathrm{T}} \boldsymbol{H}_{j,k} \boldsymbol{p}_{k,l} = 0, (k,l) \in \{(k,l) | g_{j,i,k,l} = 0, k \in \mathcal{I}_K, l \in \mathcal{I}_{L_k}\}. \tag{28}$$

Note that there are M antennas in each BS and thus M aligned directions. Due to channel randomness, the M aligned directions are linearly independent with high probability. Thus, the nulling in (28) is always feasible, i.e., there exist $\{\boldsymbol{f}_{j,i}\}$ such that Criterion 3 is met.

Then, $\boldsymbol{t}_{j,i}$ can be represented as

$$\boldsymbol{t}_{j,i}^{\mathrm{T}} = \sum_{(k,l) \in \{(k,l): g_{j,i,k,l} \neq 0\}} \boldsymbol{f}_{j,i}^{\mathrm{T}} \boldsymbol{H}_{j,k} \boldsymbol{p}_{k,l} \frac{\boldsymbol{c}_{k,l}^{\mathrm{T}}}{\sigma_{\mathrm{s},k,l}} + \tilde{\boldsymbol{z}}_{j,i}^{\mathrm{T}} \tag{29a}$$

$$= \tilde{\boldsymbol{t}}_{j,i}^{\mathrm{T}} + \tilde{\boldsymbol{z}}_{j,i}^{\mathrm{T}} \tag{29b}$$

where

$$\tilde{\boldsymbol{t}}_{j,i} = \sum_{(k,l) \in \{(k,l): g_{j,i,k,l} \neq 0\}} \boldsymbol{f}_{j,i}^{\mathrm{T}} \boldsymbol{H}_{j,k} \boldsymbol{p}_{k,l} \frac{\boldsymbol{c}_{k,l}}{\sigma_{\mathrm{s},k,l}}, \tag{30}$$

and $\tilde{\boldsymbol{z}}_{j,i} = \boldsymbol{Z}_j^{\mathrm{T}} \boldsymbol{f}_{j,i}$ where element of $\tilde{\boldsymbol{z}}_{j,i}$ follows the Gaussian distribution $\mathcal{N}(0, \sigma_z^2)$.

Example 2: We continue with Example 1. From (28), $\boldsymbol{f}_{1,1}$ is required to satisfy

$$\boldsymbol{f}_{1,1}^{\mathrm{T}} \boldsymbol{H}_{1,1} \boldsymbol{p}_{1,2} = 0 \quad \text{and } \boldsymbol{f}_{1,1}^{\mathrm{T}} \boldsymbol{H}_{1,1} \boldsymbol{p}_{1,3} = 0. \tag{31}$$

Then, we see that

$$\boldsymbol{t}_{1,1}^{\mathrm{T}} = \boldsymbol{f}_{1,1}^{\mathrm{T}} \boldsymbol{H}_{1,1} \boldsymbol{p}_{1,1} \boldsymbol{c}_{1,1}^{\mathrm{T}} + \boldsymbol{f}_{1,1}^{\mathrm{T}} \boldsymbol{H}_{1,2} \boldsymbol{p}_{2,1} \boldsymbol{c}_{2,1}^{\mathrm{T}} + \tilde{\boldsymbol{z}}_{1,1}^{\mathrm{T}}. \tag{32}$$

We see that $\boldsymbol{t}_{1,1}$ only contains the aligned spatial streams specified by $\boldsymbol{g}_{1,1}$. □

3) DECODING AT BSS

In the network-coded decoding step, BS j decodes the network-coded messages $\boldsymbol{u}_{j,i} = \boldsymbol{B}\varphi(\boldsymbol{g}_{j,i})$ from $\boldsymbol{t}_{j,i}$ for $i = 1, \cdots, L_j'$. Note that (30) can be represented by

$$\tilde{\boldsymbol{t}}_{j,i} = \sum_{(k,l) \in \{(k,l): g_{j,i,k,l} \neq 0\}} g_{j,i,k,l} \frac{\boldsymbol{f}_{j,i}^{\mathrm{T}} \boldsymbol{H}_{j,k} \boldsymbol{p}_{k,l}}{g_{j,i,k,l} \sigma_{\mathrm{s},k,l}} \boldsymbol{c}_{k,l}, \tag{33}$$

where $\frac{\boldsymbol{f}_{j,i}^{\mathrm{T}} \boldsymbol{H}_{j,k} \boldsymbol{p}_{k,l}}{g_{j,i,k,l} \sigma_{\mathrm{s},k,l}} \boldsymbol{c}_{k,l}$ is referred to as a *scaled lattice codeword* (i.e., a scaled version of $\boldsymbol{c}_{k,l}$), constructed from the scaled lattice pair

$$\left(\frac{\boldsymbol{f}_{j,i}^{\mathrm{T}} \boldsymbol{H}_{j,k} \boldsymbol{p}_{k,l}}{g_{j,i,k,l} \sigma_{\mathrm{s},k,l}} \Lambda_{c,k,l}, \frac{\boldsymbol{f}_{j,i}^{\mathrm{T}} \boldsymbol{H}_{j,k} \boldsymbol{p}_{k,l}}{g_{j,i,k,l} \sigma_{\mathrm{s},k,l}} \Lambda_{s,k,l} \right).$$

We apply the following decoding operation to $\boldsymbol{t}_{j,i}$:

$$\hat{\boldsymbol{t}}_{j,i} = Q_{\Lambda_{F,j,i}}(\boldsymbol{t}_{j,i}) \bmod \Lambda_1 \tag{34}$$

where $Q_\Lambda(\cdot)$ represents a quantization operation over lattice Λ and $\Lambda_{F,j,i}$ is the finest lattice among the scaled coding lattice $\left\{ \frac{\boldsymbol{f}_{j,i}^{\mathrm{T}} \boldsymbol{H}_{j,k} \boldsymbol{p}_{k,l}}{g_{j,i,k,l} \sigma_{\mathrm{s},k,l}} \Lambda_{c,k,l} | g_{j,i,k,l} \neq 0 \right\}$ (Here, they are assumed to be nested. A Criteria is proposed to ensure the assumption in the following). Then, by mapping $\hat{\boldsymbol{t}}_{j,i}$ (a lattice point in $\Lambda_{\mathrm{F},j,i}$) to the finite field $\mathbb{F}_q^{sk}$ [20], we obtain $\hat{\boldsymbol{u}}_{j,i}$ (a estimation of $\boldsymbol{u}_{j,i}$).

For the reliable decoding of $\boldsymbol{u}_{j,i}$, i.e. $\Pr(\hat{\boldsymbol{u}}_{j,i} \neq \boldsymbol{u}_{j,i}) \to 0$ as $n \to \infty$, we require that the decoding procedure in (34) is reliable, i.e.

$$P_e = \Pr(\hat{\boldsymbol{t}}_{j,i} \neq \tilde{\boldsymbol{t}}_{j,i}) \to 0 \quad \text{as } n \to \infty, \tag{35}$$

and $\{\tilde{\boldsymbol{t}}_{j,i}\}$ are valid lattice codewords.

The decoding error of $\tilde{\boldsymbol{t}}_{j,i}$ is equivalent to $P_e = \Pr(\tilde{\boldsymbol{z}}_{j,i} \notin \mathcal{V}_{F,j,i})$ where $\mathcal{V}_{F,j,i}$ is the Voronoi region of $\Lambda_{F,j,i}$ [21]. From Construction A, the coding lattices $\{\Lambda_{c,k,l}\}$ are Poltyrev-good and Rogers-good simultaneously, and so are $\{\Lambda_{F,j,i}\}$. Thus, the error probability P_e decays exponentially in n if [11]

$$\frac{(\mathrm{Vol}(\mathcal{V}_{F,j,i}))^{\frac{2}{n}}}{\sigma_z^2} > 2\pi e \tag{36}$$

or equivalently

$$\sigma_{\Lambda_{F,j,i}}^2 > \sigma_z^2 \tag{37}$$

where σ_z^2 is the second moment of elements of $\tilde{\boldsymbol{z}}_{j,i}$, $\mathrm{Vol}(\cdot)$ is the volume of a Voronoi region [11]. That is, $\lim_{n \to \infty} P_e = 0$ if (37) is satisfied.

To guarantee that $\{\tilde{\boldsymbol{t}}_{j,i}\}$ are network-coded codewords with combining coefficients $\{g_{j,i,k,l}\}$, it suffices to require that the following design criterion holds.

Criterion 4: For any $j \in \mathcal{I}_J$ and $i \in \mathcal{I}_{L'_j}$, the scaling coefficients

$$\left\{ \frac{\boldsymbol{f}_{j,i}^{\mathrm{T}} \boldsymbol{H}_{j,k} \boldsymbol{p}_{k,l}}{g_{j,i,k,l}\sigma_{\mathrm{s},k,l}}, \text{ for } (k,l) \text{ satisfying } g_{j,i,k,l} \neq 0 \right\} \tag{38}$$

are equal.

To meet the criterion, we need to carefully design the nested lattice chain and linear precoding matrices $\{\boldsymbol{P}_k\}$ and $\{\boldsymbol{F}_j\}$. Detailed discussions are presented in Section IV-B.

Remark 4: Note that this design criterion ensures the success of network coding with matrix $\boldsymbol{G}$. The criterion is naturally satisfied in original SSA-PNC since common shaping lattice is used (i.e., $\{\sigma_{\mathrm{s},k,l}\}$ are equal for all k, l) and the power ratios of the aligned spatial streams are the corresponding network-coding coefficient ratios (as stated in Remark 3).

D. CU DECODING

Denote the computed network-coded messages of all J BSs as $\hat{\boldsymbol{U}} = [\hat{\boldsymbol{U}}_1^{\mathrm{T}}, \hat{\boldsymbol{U}}_2^{\mathrm{T}}, \cdots, \hat{\boldsymbol{U}}_J^{\mathrm{T}}]$. CU receives the decoded network-coded messages $\hat{\boldsymbol{U}}$ with vanishing error provided that (4) is met. Then, with invertible $\varphi(\boldsymbol{G})$, the CU recovers all user messages by

$$\hat{\boldsymbol{B}} = \hat{\boldsymbol{U}}\varphi(\boldsymbol{G})^{-1}. \tag{39}$$

Under the assumption that $\hat{\boldsymbol{U}} = \boldsymbol{U}$, we have

$$\begin{aligned} H(\hat{\boldsymbol{U}}_1, \hat{\boldsymbol{U}}_2, \cdots, \hat{\boldsymbol{U}}_J) &= H(\boldsymbol{U}_1, \boldsymbol{U}_2, \cdots, \boldsymbol{U}_J) && \text{(40a)} \\ &= H(\boldsymbol{B}_1, \boldsymbol{B}_2, \cdots, \boldsymbol{B}_K) && \text{(40b)} \\ &= n\sum_{i=1}^{K} R_k && \text{(40c)} \end{aligned}$$

where (40b) follows from the bijective mapping $\boldsymbol{U} = \boldsymbol{B}\varphi(\boldsymbol{G})$ (since $\varphi(\boldsymbol{G})$ is invertible). Thus, (4) can be rewritten as

$$\sum_{k=1}^{K} R_k < C_{\mathrm{BH}}. \tag{41}$$

E. ACHIEVABLE RATES

Based on the discussions in the preceding subsections, we obtain the following main result.

Theorem 1: For a given D-MIMO system with parameters $\{\boldsymbol{P}_k\}$, $\{\beta_{j,m,k,l}\}$, $\{\boldsymbol{F}_j\}$, and the nested lattice chain $\mathcal{L}$, a rate tuple $(R_1, R_2, \cdots, R_K)$ is achievable if Criteria $1-4$ are met and

$$\sum_{k=1}^{K} R_k < C_{\mathrm{BH}} \tag{42}$$

$$R_{k,l} < \frac{1}{2} \min_{(j,i):g_{j,i,k,l}\neq 0} \log^+\left(\frac{|\boldsymbol{f}_{j,i}\boldsymbol{H}_{j,k}\boldsymbol{p}_{k,l}|^2}{g_{j,i,k,l}^2\sigma_z^2} \right), \tag{43}$$

$$\text{for } k \in \mathcal{I}_K, \quad l \in \mathcal{I}_{L_k} \tag{44}$$

where $R_k = \sum_{l=1}^{L_k} R_{k,l}$.

Proof: From the previous discussions, we see that a rate tuple $(R_1, R_2, \cdots, R_k)$ is achievable if criteria $1-4$ together (37) and (41) are met. Clearly, (42) is the same as (41). Thus, we only need to show that (44) is equivalent to (37).

We first show that (37) implies (44). To see this, we have

$$\begin{aligned} R_{k,l} &= \frac{1}{n}\log\frac{\mathrm{Vol}(\Lambda_{s,k,l})}{\mathrm{Vol}(\Lambda_{c,k,l})} && \text{(45a)} \\ &= \frac{1}{n}\log\frac{\mathrm{Vol}\left(\frac{\boldsymbol{f}_{j,i}^{\mathrm{T}}\boldsymbol{H}_{j,k}\boldsymbol{p}_{k,l}}{\sigma_{\mathrm{s},k,l}g_{j,i,k,l}}\Lambda_{s,k,l}\right)}{\mathrm{Vol}\left(\frac{\boldsymbol{f}_{j,i}^{\mathrm{T}}\boldsymbol{H}_{j,k}\boldsymbol{p}_{k,l}}{\sigma_{\mathrm{s},k,l}g_{j,i,k,l}}\Lambda_{c,k,l}\right)} && \text{(45b)} \\ &= \frac{1}{2}\log^+\left(\frac{|\boldsymbol{f}_{j,i}\boldsymbol{H}_{j,k}\boldsymbol{p}_{k,l}|^2}{g_{j,i,k,l}^2\tilde{\sigma}_{\Lambda_{c,k,l}}^2}\right) && \text{(45c)} \\ &\leq \frac{1}{2}\min_{(j,i):g_{j,i,k,l}\neq 0}\log^+\left(\frac{|\boldsymbol{f}_{j,i}\boldsymbol{H}_{j,k}\boldsymbol{p}_{k,l}|^2}{g_{j,i,k,l}^2\sigma_{\Lambda_{F,j,i}}^2}\right) && \text{(45d)} \\ &< \frac{1}{2}\min_{(j,i):g_{j,i,k,l}\neq 0}\log^+\left(\frac{|\boldsymbol{f}_{j,i}\boldsymbol{H}_{j,k}\boldsymbol{p}_{k,l}|^2}{g_{j,i,k,l}^2\sigma_z^2}\right), && \text{(45e)} \\ & \quad \text{for } k \in \mathcal{I}_K, \quad l \in \mathcal{I}_{L_k}. && \text{(45f)} \end{aligned}$$

where $\tilde{\sigma}_{\Lambda_{c,k,l}}^2$ in (45c) is the second moment of the scaled lattice $\frac{\boldsymbol{f}_{j,i}^{\mathrm{T}}\boldsymbol{H}_{j,k}\boldsymbol{p}_{k,l}}{\sigma_{\mathrm{s},k,l}g_{j,i,k,l}}\Lambda_{c,k,l}$, $\frac{|\boldsymbol{f}_{j,i}\boldsymbol{H}_{j,k}\boldsymbol{p}_{k,l}|^2}{g_{j,i,k,l}^2}$ is the second moment of $\frac{\boldsymbol{f}_{j,i}^{\mathrm{T}}\boldsymbol{H}_{j,k}\boldsymbol{p}_{k,l}}{\sigma_{\mathrm{s},k,l}g_{j,i,k,l}}\Lambda_{s,k,l}$, (45d) follows from $\tilde{\sigma}_{\Lambda_{c,k,l}}^2 \geq \sigma_{\Lambda_{F,j,i}}^2$ since $\Lambda_{F,j,i}$ is the finest lattice among the scaled coding lattices $\{\frac{\boldsymbol{f}_{j,i}^{\mathrm{T}}\boldsymbol{H}_{j,k}\boldsymbol{p}_{k,l}}{g_{j,i,k,l}}\Lambda_{c,k,l} | g_{j,i,k,l} \neq 0\}$, and (45f) is from (37).

We next show that (44) implies (37). We first note that (45a)-(45c) still hold. Combining (44) and (45c), we obtain that for any $k \in \mathcal{I}_K$ and $l \in \mathcal{I}_{L_k}$,

$$\tilde{\sigma}_{\Lambda_{c,k,l}}^2 > \sigma_z^2, \quad \text{for } (j,i) \text{ satisfying } g_{j,i,k,l} \neq 0. \tag{46}$$

Equivalently, for any $j \in \mathcal{I}_J$, $i \in \mathcal{I}_{L'_j}$,

$$\tilde{\sigma}_{\Lambda_{c,k,l}}^2 > \sigma_z^2, \quad \text{for } (k,l) \text{ satisfying } g_{j,i,k,l} \neq 0. \tag{47}$$

$\Lambda_{F,j,i}$ is finest lattice among the scaled coding lattices $\{\frac{\boldsymbol{f}_{j,i}^{\mathrm{T}}\boldsymbol{H}_{j,k}\boldsymbol{p}_{k,l}}{g_{j,i,k,l}}\Lambda_{c,k,l} | g_{j,i,k,l} \neq 0\}$. Thus, (37) holds, which concludes the proof. □

F. FURTHER DISCUSSIONS

We now highlight the differences between our approach and the approach in [12]. Basically, we generalize the original SSA-PNC by allowing different shaping lattices for the construction of nested lattice codes at the sources. This generalization, on one hand, relaxes the coefficients $\{\beta_{j,m,k,l}\}$ to be arbitrary real numbers, which allows more freedom in the design of nested lattice codes to fit the channel conditions. (In contrast, in the original SSA-PNC, $\{\beta_{j,m,k,l}\}$ are determined by the generator matrix $\tilde{\boldsymbol{G}}$.) On the other hand, in G-SSA-PNC, the SSA pattern imposes new constraints (i.e. criterion 4) on the construction of nested lattices.

This implies a necessity for the joint design of the SSA pattern and nested lattice coding, while the two can be designed sequentially in two separate steps in the original SSA-PNC. In the following, we consider the system design based on Criteria 1-4.

IV. FEASIBILITY CONDITIONS OF THE GENERALIZED SSA-PNC

In this section, we consider the feasibility of the generalized SSA-PNC approach. The discussion of feasibility consists of two parts, the feasibility of SSA precoding and the feasibility of PNC. In the subsequent, we first present the feasibility condition of SSA. After that, the feasibility condition of PNC operation is derived based on nested lattice coding.

A. FEASIBILITY OF SSA PRECODING

We now present the feasible region of precoding matrices. We first stack all precoding vectors together as

$$\tilde{\boldsymbol{p}} = [\boldsymbol{p}_{1,1}^{\mathrm{T}}, \boldsymbol{p}_{1,2}^{\mathrm{T}}, \cdots, \boldsymbol{p}_{1,L_1}^{\mathrm{T}}, \boldsymbol{p}_{2,1}^{\mathrm{T}}, \cdots, \boldsymbol{p}_{2,L_2}^{\mathrm{T}}, \cdots, \boldsymbol{p}_{K,L_K}^{\mathrm{T}}]^{\mathrm{T}}. \tag{48}$$

Then, we can represent (14) as

$$[\boldsymbol{0}, \cdots, \beta_{j,m,k_1,l_1}\boldsymbol{H}_{j,k_1}, \cdots, -\beta_{j,m,k_2,l_2}\boldsymbol{H}_{j,k_2}, \cdots, \boldsymbol{0}]\tilde{\boldsymbol{p}} = \boldsymbol{0} \quad \text{for any } l_1 \in \mathcal{S}(\boldsymbol{g}_{j,m,k_1}), l_2 \in \mathcal{S}(\boldsymbol{g}_{j,m,k_2}). \tag{49}$$

Note that $|\mathcal{S}(\boldsymbol{g}_{j,m})|$ represents the number of spatial streams aligned in the m-th direction of BS j. We see that, for given j and m, there are $|\mathcal{S}(\boldsymbol{g}_{j,m})| - 1$ independent equations in (49). Then, for $j \in \mathcal{I}_J, m \in \mathcal{I}_M$, there are

$$\sum_{j=1}^{J}\sum_{m=1}^{M}(|\mathcal{S}(\boldsymbol{g}_{j,m})| - 1) = J(L - M)$$

equations in total, where $\sum_{i=1}^{M}|\mathcal{S}(\boldsymbol{g}_{j,i})| = L$ follows from the discussions below (16). Those $J(L - M)$ equations can be stacked together, yielding

$$\tilde{\boldsymbol{H}}\tilde{\boldsymbol{p}} = \boldsymbol{0} \tag{50}$$

where $\tilde{\boldsymbol{H}} \in \mathbb{R}^{J(L-M)\times LN}$. Thus, for given $\tilde{\boldsymbol{G}}$ and $\{\beta_{j,m,k,l}\}$, the feasible region of $\tilde{\boldsymbol{p}}$ is given by the nullspace of $\tilde{\boldsymbol{H}}$. Then, a sufficient condition to ensure a non-trivial nullspace of $\tilde{\boldsymbol{H}}$ is given by

$$LN > J(L - M)M. \tag{51}$$

B. FEASIBILITY OF NETWORK-CODED DECODING

Recall from (30) that $\tilde{\boldsymbol{t}}_{j,i}$ is a sum of scaled lattice codewords with scaling factors $\{\boldsymbol{f}_{j,i}^{\mathrm{T}}\boldsymbol{H}_{j,k}\boldsymbol{p}_{k,l}\}$. To meet Criterion 4, the nested lattice chain need to be carefully designed.

We start with some basic concepts to facilitate our discussions. A *graph* consists of two finite sets, V and E. Each element in V is called a *vertex*. Each element in E is called an *edge* which is an unordered pair of vertexes. Denote by $e(v, w)$ the edge connecting vertices v and w. A *path* is a sequence of distinct vertices $v_1, v_2, \cdots, v_k$ together with their connecting edges $e(v_i, v_{i+1}) \in E$ for $i \in \mathcal{I}_{k-1}$. A *cycle* $o \triangleq (v_1, v_2, \cdots, v_k)$ is a closed path, i.e., a path $v_1, v_2, \cdots, v_k$ together with $e(v_k, v_1) \in E$. A *bipartite graph* is a graph whose vertices set is divided into two disjoint sets $\boldsymbol{V}_1$ and $\boldsymbol{V}_2$ such that each edge connects a vertex in $\boldsymbol{V}_1$ to a vertex in $\boldsymbol{V}_2$.

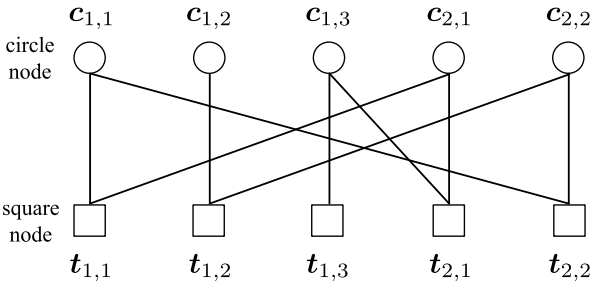

FIGURE 3. Bipartite graph of G where $G_1 = [g_{1,1}, g_{1,2}, g_{1,3}]^{\mathrm{T}}$ and $G_2 = [g_{2,1}, g_{2,2}]^{\mathrm{T}}$ with indicator vectors in Example 1.

We now construct a bipartite graph to express the relation between $\{\boldsymbol{c}_{k,l}\}$ and the $\{\boldsymbol{t}_{j,i}\}$. We represent $\{\boldsymbol{c}_{k,l}\}$ as the circle node set and $\{\boldsymbol{t}_{j,i}\}$ as the square node set. Each edge $e(\boldsymbol{c}_{k,l}, \boldsymbol{t}_{j,i})$ means that $\boldsymbol{t}_{j,i}$ contains the spatial stream $\boldsymbol{c}_{k,l}$. Consider example 1 (illustrated in Fig. 2). The corresponding bipartite graph is given in Fig. 3. The fact that $\boldsymbol{t}_{1,1}$ is connected to $\boldsymbol{c}_{1,1}$ and $\boldsymbol{c}_{2,1}$ indicates that $\boldsymbol{c}_{1,1}$ and $\boldsymbol{c}_{2,1}$ are aligned at BS 1 (see the SSA in the dashed box of Fig. 2) and the two aligned streams generates $\boldsymbol{t}_{1,1}$ (as expressed by (32)). We are now ready to present the feasibility condition of a nested lattice chain for network-coded decoding.

1) CYCLE-FREE BIPARTITE GRAPH

We first consider the case of bipartite graphs with no cycle. We show the existence of a nested lattice chain $\mathcal{L}$ such that Criterion 4 is met.

Theorem 2: Assume that $\{\boldsymbol{p}_{k,l}\}$, $\{\boldsymbol{f}_{j,i}\}$, *and* $\boldsymbol{G}$ *satisfy Criteria* $1 - 3$. *If no cycle exists in the bipartite graph associated with* $\boldsymbol{G}$, *then there always exists a nested lattice chain* $\mathcal{L}$ *such that Criterion 4 is met.*

The proof of Theorem 2 is presented at Appendix A.

Example 3: Consider the bipartite graph in Fig. 3. Since there is no cycle in the bipartite graph, the graph can be represented into a tree. We next show the procedure of design $\{\sigma_{\mathrm{s},k,l}\}$ for given $\{\boldsymbol{p}_{k,l}\}$, $\{\boldsymbol{f}_{j,i}\}$, $\boldsymbol{G}$, and $\boldsymbol{H}$.

By applying the broad first search on the graph in 3, we can see that the set of child nodes of $\boldsymbol{c}_{1,1}$ (i.e., the square nodes connected to $\boldsymbol{c}_{1,1}$) are $\{\boldsymbol{t}_{1,1}, \boldsymbol{t}_{2,2}\}$. Note that $\boldsymbol{c}_{1,1}$ is connected to and $\boldsymbol{t}_{2,2}$. Let the second moment of $\Lambda_{s,1,1}$ be $\sigma_{\mathrm{s},1,1} = 1$. Note that the child node of $\boldsymbol{t}_{1,1}$ is $\boldsymbol{c}_{2,1}$. Thus, we design $\sigma_{\mathrm{s},2,1}$ to satisfy

$$\frac{\boldsymbol{f}_{1,1}^{\mathrm{T}}\boldsymbol{H}_{1,1}\boldsymbol{p}_{1,1}}{g_{1,1,1,1}^2\sigma_{\mathrm{s},1,1}} = \frac{\boldsymbol{f}_{1,1}^{\mathrm{T}}\boldsymbol{H}_{1,2}\boldsymbol{p}_{2,1}}{g_{1,1,2,1}\sigma_{\mathrm{s},2,1}}.$$

Also, since the child node of $\boldsymbol{t}_{2,2}$ is $\boldsymbol{c}_{2,2}$, we design $\sigma_{\mathrm{s},2,2}$ to satisfy

$$\frac{\boldsymbol{f}_{2,2}^{\mathrm{T}}\boldsymbol{H}_{2,1}\boldsymbol{p}_{1,1}}{g_{2,2,1,1}\sigma_{\mathrm{s},1,1}} = \frac{\boldsymbol{f}_{2,2}^{\mathrm{T}}\boldsymbol{H}_{2,2}\boldsymbol{p}_{2,2}}{g_{2,2,2,2}\sigma_{\mathrm{s},2,2}}.$$

Similarly, for the remaining circle nodes $(\boldsymbol{c}_{1,2}, \boldsymbol{c}_{1,3})$, we have

$$\frac{\boldsymbol{f}_{1,2}^{\mathrm{T}}\boldsymbol{H}_{1,2}\boldsymbol{p}_{2,2}}{g_{1,2,2,2}\sigma_{\mathrm{s},2,2}} = \frac{\boldsymbol{f}_{1,2}^{\mathrm{T}}\boldsymbol{H}_{1,1}\boldsymbol{p}_{1,2}}{g_{1,2,1,2}\sigma_{\mathrm{s},1,2}},$$
$$\frac{\boldsymbol{f}_{2,1}^{\mathrm{T}}\boldsymbol{H}_{2,2}\boldsymbol{p}_{2,1}}{g_{2,1,2,1}\sigma_{\mathrm{s},2,1}} = \frac{\boldsymbol{f}_{2,1}^{\mathrm{T}}\boldsymbol{H}_{2,1}\boldsymbol{p}_{1,3}}{g_{2,1,1,3}\sigma_{\mathrm{s},1,3}}.$$

2) BIPARTITE GRAPH WITH CYCLES

We now consider the case of bipartite graphs with cycles. We start with definitions. A *cycle basis*, denoted by $\mathcal{O}$, is a maximal set of linearly independent cycles.[3] An example is illustrated in Fig. 4. Denote by $o = (\boldsymbol{c}_{k_1,l_1}, \boldsymbol{t}_{j_1,i_1}, \boldsymbol{c}_{k_2,l_2}, \boldsymbol{t}_{j_2,i_2}, \cdots, \boldsymbol{c}_{k_\gamma,l_\gamma}, \boldsymbol{t}_{j_\gamma,i_\gamma})$ a cycle in $\mathcal{O}$.

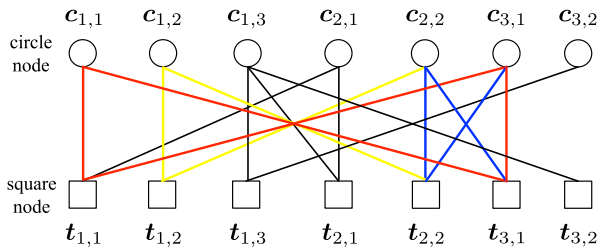

FIGURE 4. Bipartite graph with cycles. The cycle basis in the graph is given by $\mathcal{O} = \{(\boldsymbol{c}_{1,1}, \boldsymbol{t}_{1,1}, \boldsymbol{c}_{3,1}, \boldsymbol{t}_{3,1}), (\boldsymbol{c}_{3,1}, \boldsymbol{t}_{2,2}, \boldsymbol{c}_{2,2}, \boldsymbol{t}_{3,1}), (\boldsymbol{c}_{1,2}, \boldsymbol{t}_{1,2}, \boldsymbol{c}_{2,2}, \boldsymbol{t}_{2,2})\}$.

Theorem 3: Consider any given $\{\boldsymbol{p}_{k,l}\}$, $\{\boldsymbol{f}_{j,i}\}$, *and* $\boldsymbol{G}$ *satisfying Criteria* $1-3$. *Then, there always exists a nested lattice chain* $\mathcal{L}$ *such that Criterion 4 is met if* $\{\beta_{j,i,k,l}\}$ *satisfies* [4]

$$\prod_{\tau=1}^{\gamma} \beta_{j_\tau,i_\tau,k_\tau,l_\tau} g_{j_\tau,i_\tau,k_\tau,l_\tau} = \prod_{\tau=1}^{\gamma} \beta_{j_\tau,i_\tau,k_{\tau+1},l_{\tau+1}} g_{j_\tau,i_\tau,k_{\tau+1},l_{\tau+1}}, \quad \textit{for any } o = (\boldsymbol{c}_{k_1,l_1}, \boldsymbol{t}_{j_1,i_1}, \boldsymbol{c}_{k_2,l_2}, \boldsymbol{t}_{j_2,i_2}, \cdots, \boldsymbol{c}_{k_\gamma,l_\gamma}, \boldsymbol{t}_{j_\gamma,i_\gamma}) \in \mathcal{O}. \quad (52)$$

The proof of Theorem 3 is presented at Appendix B.

Example 4: We consider a D-MIMO system with $J = K = 3, N = 3, M = 6, L_1 = 3, L_2 = L_3 = 2, L_1' = 3, L_2' = L_3' = 2$. The associated bipartite graph is illustrated in Fig. 4. There are 3 cycles in the cycle basis: $o_1 = (\boldsymbol{c}_{1,1}, \boldsymbol{t}_{1,1}, \boldsymbol{c}_{3,1}, \boldsymbol{t}_{3,1})$, $o_2 = (\boldsymbol{c}_{3,1}, \boldsymbol{t}_{2,2}, \boldsymbol{c}_{2,2}, \boldsymbol{t}_{3,1})$, $o_3 = (\boldsymbol{c}_{1,2}, \boldsymbol{t}_{1,2}, \boldsymbol{c}_{2,2}, \boldsymbol{t}_{2,2})$.

From (52), the constraint for $\{\beta_{j,i,k,l}\}$ induced from cycle o_1 is given by

$$(\beta_{1,1,1,1}g_{1,1,1,1})(\beta_{3,1,3,1}g_{3,1,3,1}) = (\beta_{1,1,3,1}g_{1,1,3,1})(\beta_{3,1,1,1}g_{3,1,1,1}).$$

Similarly, in o_2 and o_3, the constraints for the two cycles are respectively given by

$$(\beta_{2,2,3,1}g_{2,2,3,1})(\beta_{3,1,2,2}g_{3,1,2,2}) = (\beta_{2,2,2,2}g_{2,2,2,2})(\beta_{3,1,3,1}g_{3,1,3,1})$$
$$(\beta_{1,2,1,2}g_{1,2,1,2})(\beta_{2,2,2,2}g_{2,2,2,2}) = (\beta_{1,2,2,2}g_{1,2,2,2})(\beta_{2,2,1,2}g_{2,2,1,2}).$$

[3] "Linearly independent" means that for any subset $\mathcal{O}' \subset \mathcal{O}$, the subgraph formed by the circles in $\mathcal{O}'$ cannot contain a cycle o satisfying $o \in \mathcal{O}$ and $o \notin \mathcal{O}'$.

[4] In (52), we set $k_{\gamma+1} = k_1$ and $l_{\gamma+1} = l_1$ for notational convenience.

V. SUM-RATE MAXIMIZATION

In this section, we consider the sum-rate maximization problem of the D-MIMO system in Fig. 1 which employs our optimized SSA-PNC scheme.

A. PROBLEM FORMULATION

For a given D-MIMO system with feasible parameters $K, J, M, N, \{L_k\}, \{L_J'\}$, and $\tilde{\boldsymbol{G}}$, the sum-rate maximization problem is given by

$$\underset{\tilde{\boldsymbol{p}},\boldsymbol{F},R_{k,l},\{\beta_{j,m,k,l}\}}{\text{maximize}} \sum_{k=1}^{K}\sum_{l=1}^{L_k} R_{k,l} \quad (53a)$$

$$\text{subject to } R_{k,l} < \min_{(j,i):g_{j,i,k,l}\neq 0} \log^{+}\left(\frac{|\boldsymbol{f}_{j,i}\boldsymbol{H}_{j,k}\boldsymbol{p}_{k,l}|^2}{\sigma_z^2}\right), \quad \text{for } k \in \mathcal{I}_K, \quad l \in \mathcal{I}_{L_k} \quad (53b)$$

$$\sum_{k=1}^{K}\sum_{l=1}^{L_k} R_{k,l} < C_{\mathrm{BH}} \quad (53c)$$

$$\mathrm{tr}(\boldsymbol{P}_k\boldsymbol{P}_k^{\mathrm{T}}) \le P_k, \quad \text{for } k \in \mathcal{I}_K \quad (53d)$$

$$\tilde{\boldsymbol{H}}\tilde{\boldsymbol{p}} = \boldsymbol{0} \text{ with } \tilde{\boldsymbol{p}} \text{ in (48)} \quad (53e)$$

$$\boldsymbol{f}_{j,i}^{\mathrm{T}}\boldsymbol{H}_{j,k}\boldsymbol{p}_{k,l} = 0, \quad \text{for } (j,i,k,l) \text{ satisfying } g_{j,i,k,l} \neq 0 \quad (53f)$$

$$\|\boldsymbol{f}_{j,i}\| = 1 \quad (53g)$$

$$|\beta_{j,m,k,l}| \in \mathbb{R}^{++} \text{satisfying(52)}. \quad (53h)$$

In the above formulation, (53d) and (53e) are the constraints to precoding matrices, and are respectively from (11) and (50); (53f) and (53g) are respectively from Criteria 3 and (28); (53h) is from Theorem 3.

B. APPROXIMATE SOLUTION

The sum-rate maximization problem is highly non-convex and difficult to obtain the optimal solution because of the non-convex form of (53b) and the integer programming for the optimization of $\tilde{\boldsymbol{G}}$. Here we present an approximate solution with a heuristic method. For given $\{\beta_{j,m,k,l}\}$ satisfying (53h), we can solve (53) by the following steps:

- Construct $\tilde{\boldsymbol{H}}$ and obtain an arbitrary basis of the nullspace of $\tilde{\boldsymbol{H}}$;
- Generate a feasible $\tilde{\boldsymbol{p}}$ in the nullspace of $\tilde{\boldsymbol{H}}$ using the basis obtained in the first step;
- With $\tilde{\boldsymbol{p}}$, generate feasible $\{\boldsymbol{f}_{j,i}\}$ satisfying (53f) and (53g);
- Calculate $R_{k,l}$ using the upper bound in (53b).

Note that the dimension of the nullspace of $\tilde{\boldsymbol{H}}$ is $LN - J(L-M)M$. Thus, the coefficient tuple of $\tilde{\boldsymbol{p}}$ consists of $K_p \triangleq LN - J(L-M)M$ elements, denoted by $(\alpha_1, \alpha_2, \cdots, \alpha_{K_p})$ with $\alpha \in \mathbb{R}$. Similarly, generate the basis of feasible region of $\boldsymbol{f}_{j,i}$ according (53f) and generate the coefficient

tuple $(\theta_1, \theta_2, \cdots, \theta_{K_f})$. Thus, we obtain a feasible $\boldsymbol{f}_{j,i}$. What remains is how to optimize $\{\beta_{j,m,k,l}\}$, and the two coefficient tuples. In this paper, we apply the differential evolution algorithm [22]. The algorithm is practical in such a non-convex and multi-variable problem.

Therefore, with given $\boldsymbol{H}$ and $\boldsymbol{G}$, we utilize the differential evolution algorithm to obtain suboptimal candidates, i.e., $\{\{\beta\}, (\alpha_1, \alpha_2, \cdots, \alpha_{K_\alpha})\}, (\theta_1, \theta_2, \cdots, \theta_{K_f})$. The corresponding maximal sum rate is given by Algorithm 1.

Algorithm 1

Require: $\boldsymbol{H}, \tilde{\boldsymbol{G}}, \{\beta_{j,m,k,l}\}, \quad (\alpha_1, \alpha_2, \cdots, \alpha_{K_\alpha}), (\theta_1, \theta_2, \cdots, \theta_{K_f})$.

Ensure: $\sum_{l=1}^{L} R_{i,l}$.

1: For given $\{\beta_{j,m,k,l}\}$, $\tilde{\boldsymbol{G}}$, and $\boldsymbol{H}$, construct $\tilde{\boldsymbol{H}}$ in (50).
2: Obtain a basis of nullspace of $\tilde{\boldsymbol{H}}$ by SVD and generate $\tilde{\boldsymbol{p}}$ with coefficient tuple $(\alpha_1, \alpha_2, \cdots, \alpha_{K_\alpha})$.
3: Obtain the basis of feasible region of $\boldsymbol{f}_{j,i}$ from (53f) and generate a feasible $\boldsymbol{f}_{j,i}$ with $(\theta_1, \theta_2, \cdots, \theta_{K_f})$. Scale $\boldsymbol{f}_{j,i}$ to satisfy (53g).
4: Calculate the upper bound of $R_{i,l}$ in (53b) and output $\sum_{l=1}^{L} R_{i,l}$.

C. OPTIMIZATION OF $\tilde{G}$

The optimization procedures above is based on a fixed generator matrix $\tilde{\boldsymbol{G}}$. Since $\tilde{\boldsymbol{G}}$ determines the pattern of SSA, for given channel matrix, various alignment patterns result into various performances of our G-SSA-PNC scheme. Not strictly, the pattern should be "close" to the channel matrix in some senses. However, up to now, we don't know how to measure the "closeness" between $\tilde{\boldsymbol{G}}$ and channel matrix. Besides, it is NP-hard to optimize such a matrix with discrete values.

In this paper, we apply the brute-force method to search an optimal $\tilde{\boldsymbol{G}}$ (each element in $\tilde{\boldsymbol{G}}$ is set to be 0 or 1). Though with high computation complexity, the method can show the essential performance gain of optimizing $\tilde{\boldsymbol{G}}$.

VI. NUMERICAL RESULTS

In this section, we apply the proposed scheme to the D-MIMO systems with different parameters. In the simulations, the power budgets of the users satisfy $P_1 = P_2 = \cdots = P_K = P$ and the SNR at transmitter is given by $\text{SNR} \triangleq \frac{P}{\sigma^2}$. The numerical results are obtained by averaging over 2000 channel realizations.

A. PERFORMANCE OF GENERALIZED SSA-PNC

In this subsection, we show the performances of the proposed G-SSA-PNC scheme. Specifically, to show the advantage of the generalizations in G-SSA-PNC, we consider the performance comparison between the following four schemes:

- SSA-PNC: the original SSA-PNC scheme in [12];
- G-SSA-PNC-P: the proposed scheme with optimized precoding matrix $\{\boldsymbol{P}_k\}$ ($\{\beta_{j,m,k,l}\}$ are all set to 1);
- G-SSA-PNC-P&β: the proposed scheme with optimized precoding matrix $\{\boldsymbol{P}_k\}$ and $\{\beta_{j,m,k,l}\}$;
- G-SSA-PNC-P&β&G: the proposed scheme with optimized precoding matrix $\{\boldsymbol{P}_k\}$, β, and generator matrix $\tilde{\boldsymbol{G}}$;

In the first three schemes, the integer vectors are given in Example 1 and the corresponding generator matrix is given by (18).

1) CHANNEL MODEL WITH RAYLEIGH FADING

We assume each element in $\{\boldsymbol{H}_{j,k}\}$ satisfies i.i.d. normal distribution, i.e. $\boldsymbol{H}_{j,k} \sim \mathcal{N}(\boldsymbol{0}, \boldsymbol{I})$ for each j, k. The corresponding numerical results are given in Figs. 5 and 6.

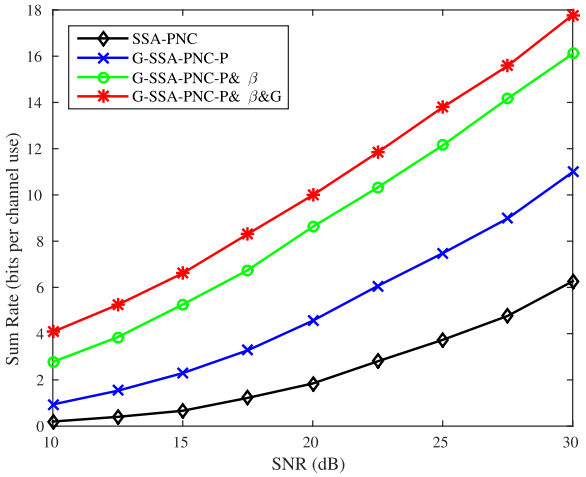

FIGURE 5. Simulation results for $K = J = 2, N = 3, M = 3$ with Rayleigh fading.

Fig. 5 shows the result of the sum rate versus SNR of G-SSA-PNC under a D-MIMO system with $K = J = 2, N = M = 3, L = 5, C_B = \frac{L}{2} \log \frac{K\text{SNR}}{L}$. We see that with optimized precoding matrix $\boldsymbol{P}$, the performance gain over original SSA-PNC is about 7 dB in high SNR. By optimizing $\{\beta\}$, there is an extra 7 dB. By optimizing $\tilde{\boldsymbol{G}}$ additionally, there is about a 2 dB extra gain.

Fig. 6 shows the result of the sum rate versus SNR of G-SSA-PNC under a D-MIMO system with $K = J = 3, N = 6, M = 3, L = 7$, and $C_B = \frac{L}{2} \log \frac{K\text{SNR}}{L}$. Similar to Fig. 5, considerable gains are obtained by optimizing $\{\boldsymbol{P}_i\}, \{\beta\}$, and $\boldsymbol{G}$. In particular, with optimized precoding matrix $\boldsymbol{P}$, the performance gain over original SSA-PNC is more than 10 dB gain. By optimizing $\{\beta\}$ additionally, there is a 2 dB gain. By optimizing $\tilde{\boldsymbol{G}}$ additionally, there is about a 5 dB extra.

2) CHANNEL MODEL WITH PATH LOSS FADING AND SPATIAL CORRELATION

In more practical scenarios, due to the geometrical separation between BSs and users as well as the multi-antennas setting, the channel fading and spatial correlation should be considered in the channel modeling. Specifically, we factorize the

channel coefficient matrix in (2) as

$$\boldsymbol{H}_{j,k} = \frac{\boldsymbol{R}_{j,\mathrm{r}}^{\frac{1}{2}} \tilde{\boldsymbol{H}}_{j,k} (\boldsymbol{R}_{k,\mathrm{t}}^{\frac{1}{2}})^{\mathrm{T}}}{d_{j,k}^{\frac{3}{2}}} \tag{54}$$

where $\boldsymbol{R}_{j,\mathrm{r}}$ is the receiver-side spatial correlation matrix, $\boldsymbol{R}_{k,\mathrm{t}}$ is the transmitter-side spatial correlation matrix, and $d_{j,k}$ is the distance between user k and BS j in the pass loss model. Then, the channel coefficient matrix can be expressed as

$$\boldsymbol{H}_{j,k} \sim \mathcal{N}(\boldsymbol{0}, \boldsymbol{R}_t \otimes \boldsymbol{R}_r) \tag{55}$$

where $\otimes$ is the Kronecker product. Following [23], the spatial correlation matrix $\boldsymbol{R}_t$ is set as

$$\boldsymbol{R}_t = \begin{bmatrix} 1 & \alpha & \alpha^2 & \cdots & \alpha^{N-1} \\ \alpha & 1 & \alpha & \cdots & \alpha^{N-2} \\ \alpha^2 & \alpha & 1 & \cdots & \alpha^{N-3} \\ \vdots & \vdots & \vdots & \ddots & \vdots \\ \alpha^{N-1} & \alpha^{N-2} & \alpha^{N-3} & \cdots & 1 \end{bmatrix} \tag{56}$$

and $\boldsymbol{R}_r$ is the same as $\boldsymbol{R}_t$ in (56) except that the antenna number N is replaced by M. Though the simple model in (56) is not accurate for the real world antenna array, we can use it to study the effect of antenna correlation to the system performance by only manipulating α.

In our simulation, the following parameter settings are employed: $\alpha = 0.2$, $d_{j,k} \sim U(10, 100)$ in meter, and $C_B = \frac{L}{2} \log \frac{K \mathrm{SNR}}{10^{4.5} L}$. The considered SNR range is actually reasonable for practical systems with large scale fading. The simulation results for $K = J = 2$ and $K = J = 3$ are respectively presented in Fig. 7 and Fig. 8. We see that the trends of the four SSA-PNC schemes in Figs. 5 and 6 remain roughly unchanged in Figs. 7 and 8. We also see that G-SSA-PNC achieves considerable performance gains at high SNR.

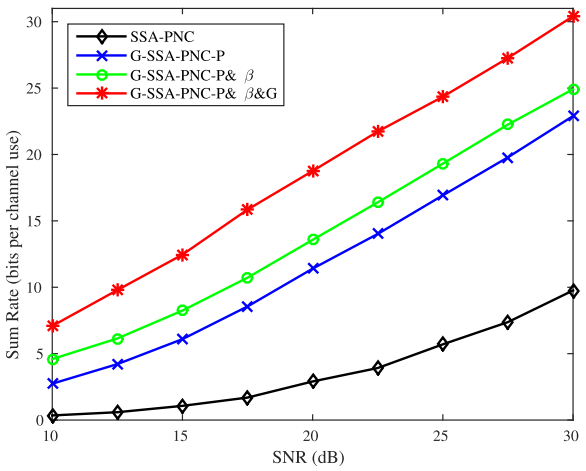

FIGURE 6. Simulation results for $K = J = 3, N = 6, M = 3$ with Rayleigh fading.

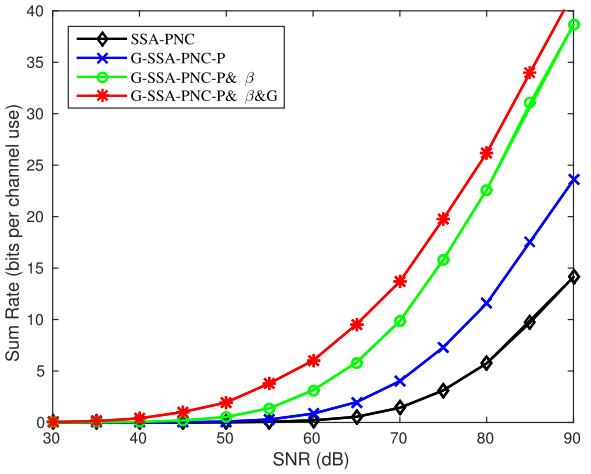

FIGURE 7. Simulation results for $K = J = 2, N = 3, M = 3$ with large scale fading.

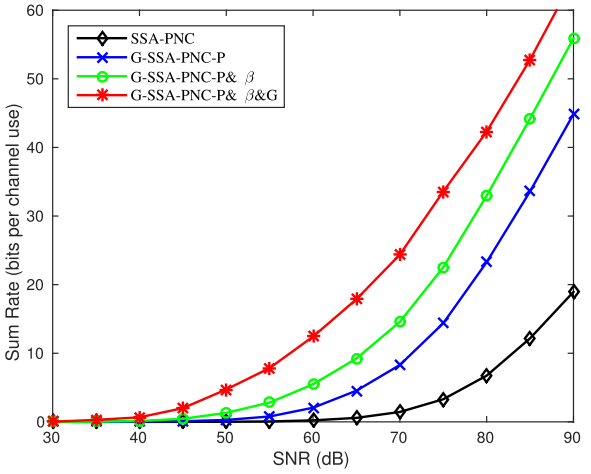

FIGURE 8. Simulation results for $K = J = 3, N = 6, M = 3$ with large scale fading.

B. PERFORMANCE COMPARISON OF BENCHMARK SCHEMES

In this subsection, we compare the proposed G-SSA-PNC with other benchmark schemes. In G-SSA-PNC, parameters $\{\boldsymbol{P}_i\}$, $\{\beta\}$, and $\tilde{\boldsymbol{G}}$ are all optimized following Algorithm 1. The other benchmark schemes are described as follows.

- IA: The interference alignment approach in [6]; no symbol extension is considered.
- GCCF: Each MIMO users is regarded as M equivalent single-antenna users, and then GCCF in [16] is applied to the equivalent single-antenna system model; all the transmit antennas in the system have the same transmission power.
- CF: Following [4], each user linearly precodes the message to be transmitted; each BSs first takes a LMMSE estimator to process its received signal and then quantize the processed signal to satisfy the capacity limit of the backhaul link; the beamforming matrix and quantization noise covariance matrices are optimized by the WMMSE-SCA method in [4].

TABLE 2. The average CPU running time of various algorithms per channel realization.

(K, J, N, M)	SSA-PNC	G-SSA-PNC-P	G-SSA-PNC-P-β	G-SSA-PNC-P-β-G
$(2, 2, 3, 3)$	0.1s	1s	10s	130s
$(3, 3, 6, 3)$	0.1s	4s	58s	over 1h

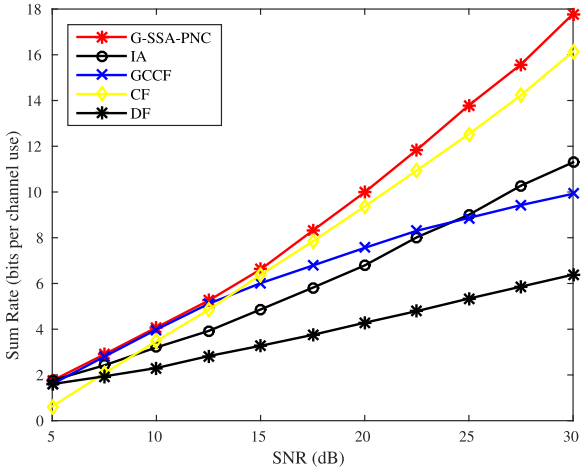

FIGURE 9. Simulation results for $K = J = 2, N = 3, M = 3$ with Rayleigh fading.

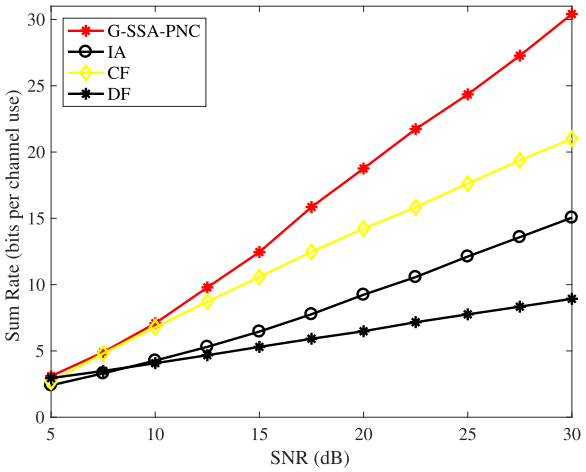

FIGURE 10. Performance comparison under SNR = 30 dB, $K = J = 2$, and $N = M = 3$.

- DF: Here we consider a straightforward decode-and-forward scheme in which each BS k is required to decode the message of user k for $k \in \mathcal{I}_K$.

1) SUM RATE VERSUS SNR UNDER LIMITED BACKHAUL CAPACITY

The numerical results are presented in Fig. 9 and Fig. 11, where Fig. 9 is under Rayleigh fading with $K = J = 2$, and Fig. 11 is under Rayleigh fading with $K = J = 3$. We see that G-SSA-PNC outperforms the benchmark schemes at relatively high SNR. GCCF is not presented in Fig. 10 due to the intractable complexity under this system setting.

2) SUM RATE VERSUS BACKHAUL CAPACITY UNDER FIXED SNR

The numerical result is given in Fig. 10 with the system parameters $K = J = 2, N = M = 3, L = 5$, and SNR = 30dB. Here the upper bound is defined as follows. Assume that the BSs can fully cooperate in decoding and forwarding. Then the D-MIMO system can be treated as a MIMO multiple-access channel. Then, an upper bound is given by $C_{\text{upper}} = \min\{R_{\text{mac}}, C_{\text{BH}}\}$, where R_{mac} is the capacity of the equivalent MIMO multiple-access channel.

When the sum backhaul capacity is small (less than 8 bits/channel use), G-SSA-PNC outperforms CF and achieves the same performance as IA, GCCF, and DF. When the sum backhaul capacity is moderate (between 8 to 24 bits/channel use), G-SSA-PNC outperforms the other four schemes. When the sum backhaul capacity is relatively large (over 24 bits/channel use), CF outperforms G-SSA-PNC. The reason is that, as the sum backhaul capacity increases, the compression operation in CF becomes information lossless, and hence eventually outperforms the other schemes.

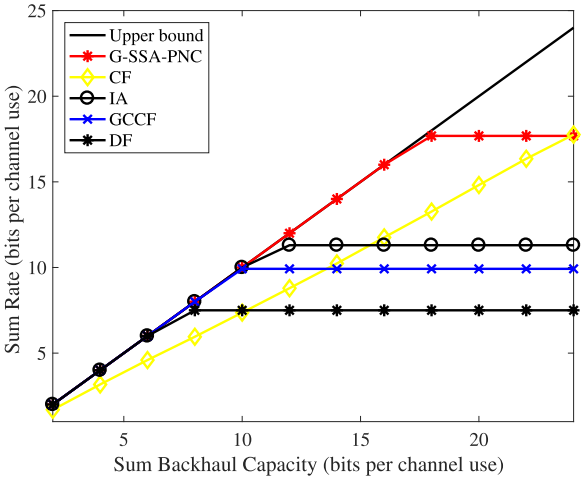

FIGURE 11. Simulation results for $K = J = 3, N = 6, M = 3$ with Rayleigh fading.

C. COMPLEXITY ISSUES

We now briefly discuss the complexity involved in G-SSA-PNC. From the discussions in Section, it is not difficult to see that the operation of G-SSA-PNC is similar to that of SSA-PNC. Thus, the operational complexity of G-SSA-PNC is comparable to that of SSA-PNC. The difference is that G-SSA-PNC involves additional optimization of SSA precoding and nested lattice coding coefficients. To see this, we present the average CPU running time of various optimization algorithms for each channel realization in Table 2. The simulation is implemented with Intel

i5-6267U and Python2.7. Due to the brute-force search of $\tilde{\boldsymbol{G}}$ as well as the heuristic search of $\{\beta_{j,m,k,l}\}$ and $\tilde{\boldsymbol{p}}$, we see that the optimization becomes more and more time-consuming as the increase of the network size and the number of optimization variables. The design of more efficient optimization algorithms is an interesting research topic, but is out of the scope of this paper.

VII. CONCLUSION

In this paper, we proposed a generalized SSA-PNC scheme for distributed MIMO systems. Compared to the original SSA-PNC scheme in [12], we improved the system performance through the following aspects. We allowed different shaping lattice for each source nested lattice code. This allows more freedom in the design of nested lattice codes to fit the channel conditions. We presented the feasibility conditions of the G-SSA-PNC scheme. We considered jointly designed the linear precoding for SSA, the generator matrix as well as the source nested lattice codes and thus formulated a sum-rate maximization problem. To show the performance of G-SSA-PNC, we addressed the non-convex maximization problem by taking an approximate approach. The numerical results demonstrate a considerable gain of our proposed SSA-PNC scheme over the benchmark schemes.

APPENDIX A
PROOF OF THEOREM 2

From [21, Theorem 2], we see that $\mathcal{L}$ always exists provided $\sigma_{\mathrm{s},k,l} > \sigma_{\mathrm{c},k,l}$ for $k \in \mathcal{I}_K, l \in \mathcal{I}_{L_k}$. Thus, to prove Theorem 2, it suffices to show the existence of $\{\sigma_{\mathrm{s},k,l}, \sigma_{\mathrm{c},k,l}\}$ such that $\sigma_{\mathrm{s},k,l} > \sigma_{\mathrm{c},k,l}$ for $k \in \mathcal{I}_K, l \in \mathcal{I}_{L_k}$ and Criterion 4 is met. Also note that Criterion 4 does not involve $\{\sigma_{\mathrm{c},k,l}\}$. That is, for any given $\sigma_{\mathrm{s},k,l}$, the design of $\sigma_{\mathrm{c},k,l}$ is irrelevant to Criterion 4. Therefore, we only need to design $\{\sigma_{\mathrm{s},k,l}\}$ to meet Criterion 4.

To this end, we apply the broad first search (BFS) algorithm to the bipartite graph associated with $\boldsymbol{G}$. Since the bipartite graph is cycle-free, BFS yields a tree if the graph is connected or a forest otherwise [24]. We next only consider the case of a tree. The discussion for a forest is similar and thus omitted.

Without the loss of generality, we assume that the first visited node (root node) in BFS is the circle node $\boldsymbol{c}_{1,1}$. The child nodes of $\boldsymbol{c}_{1,1}$ is a set of square nodes, given by

$$\mathscr{C}_{1,1} = \{\boldsymbol{t}_{j,i}, \quad \text{for } (j,i) \text{ satisfying } g_{j,i,1,1} \neq 0\}. \tag{57}$$

Further, the child nodes of each child node $\boldsymbol{t}_{j,i}$ in (57) is a set of circle nodes, given by

$$\mathcal{T}_{j,i} = \{\boldsymbol{c}_{k,l}, \quad \text{for } (k,l) \text{ satisfying } g_{j,i,k,l} \neq 0\}. \tag{58}$$

We choose $\sigma_{\mathrm{s},1,1} = 1$. To satisfy Criterion 4, for each square node $\boldsymbol{t}_{j,i} \in \mathscr{C}_{1,1}$, the following equations need to hold

$$\frac{\boldsymbol{f}_{j,i}\boldsymbol{H}_{j,k}\boldsymbol{p}_{k,l}}{g_{j,i,k,l}\sigma_{\mathrm{s},k,l}} = \frac{\boldsymbol{f}_{j,i}\boldsymbol{H}_{j,1}\boldsymbol{p}_{1,1}}{g_{j,i,1,1}\sigma_{\mathrm{s},1,1}}, \quad \text{for } (k,l) \text{ satisfying } g_{j,i,k,l} \neq 0. \tag{59}$$

That is, for each circle node $\boldsymbol{c}_{k,l} \in \mathcal{T}_{j,i}$, the corresponding $\sigma_{\mathrm{s},k,l}$ is designed to satisfy (59). By induction, for any circle node in the tree, the corresponding $\sigma_{\mathrm{s},k,l}$ is determined and only determined once following the above approach. At the same time, Criterion 4 is met since all square nodes $\{\boldsymbol{t}_{j,i}\}$ are visited. This concludes the proof.

APPENDIX B
PROOF OF THEOREM 3

Denote by $\mathcal{G}$ the bipartite graph associated with $\boldsymbol{G}$. We remove one edge in each cycle $o \in \mathcal{O}$ so that the bipartite graph $\mathcal{G}$ reduces to a cycle-free graph, denoted by $\mathcal{G}'$. Denote by $\mathcal{E}$ the set of all removed edges. Note that removing an edge $e(\boldsymbol{c}_{k,l}, \boldsymbol{t}_{j,i})$ from $\mathcal{G}$ is equivalent to forcing the non-zero integer $g_{j,i,k,l}$ in $\boldsymbol{G}$ to zero. Then, denote by $\boldsymbol{G}'$ the network-coding matrix associated with $\mathcal{G}'$. Since $\mathcal{G}'$ is cycle-free, we follow the approach in the proof of Theorem 2 to design $\{\sigma_{\mathrm{s},k,l}\}$. Hence, Criterion 4 is met for $\boldsymbol{G}'$.

However, by adding back the removed edges in $\mathcal{E}$ (i.e., recovering the zero-forced $\{g_{j,i,k,l}\}$ in $\boldsymbol{G}'$), the recovery of $\boldsymbol{G}$ from $\boldsymbol{G}'$ may violate Criterion 4. Therefore, we need to impose extra constraints to ensure Criterion 4 is still met. To prove Theorem 3, what remains is to show that with the designed $\{\sigma_{\mathrm{s},k,l}\}$, Criterion 4 is met provided that $\{\beta_{j,m,k,l}\}$ satisfies (52).

From $\boldsymbol{G}$, we obtain the cycle basis in $\mathcal{G}$ [24]. Consider a cycle $o = (\boldsymbol{c}_{k_1,l_1}, \boldsymbol{t}_{j_1,i_1}, \boldsymbol{c}_{k_2,l_2}, \boldsymbol{t}_{j_2,i_2}, \cdots, \boldsymbol{c}_{k_\gamma,l_\gamma}, \boldsymbol{t}_{j_\gamma,i_\gamma}) \in \mathcal{O}$. Without the loss of generality, we assume that only the edge $(\boldsymbol{c}_{k_1,l_1}, \boldsymbol{t}_{j_1,i_1})$ is removed. To meet Criterion 4, we need to guarantee that the scaling factor of the removed edge $(\boldsymbol{c}_{k_1,l_1}, \boldsymbol{t}_{j_1,i_1})$ is equal to the scaling factor of an un-removed edge $e(\boldsymbol{c}_{k,l}, \boldsymbol{t}_{j_1,i_1})$ satisfying $g_{j_1,i_1,k,l} \neq 0$. Note that $e(\boldsymbol{c}_{k_2,l_2}, \boldsymbol{t}_{j_1,i_1})$ is such an un-removed edge. Thus, the following equation need to hold

$$\frac{\boldsymbol{f}_{j_1,i_1}^{\mathrm{T}}\boldsymbol{H}_{j_1,k_1}\boldsymbol{p}_{k_1,l_1}}{g_{j_1,i_1,k_1,l_1}\sigma_{\mathrm{s},k_1,l_1}} = \frac{\boldsymbol{f}_{j_1,i_1}^{\mathrm{T}}\boldsymbol{H}_{j_1,k_2}\boldsymbol{p}_{k_2,l_2}}{g_{j_1,i_1,k_2,l_2}\sigma_{\mathrm{s},k_2,l_2}}. \tag{60}$$

From the proof of Theorem 2, we see that the following equations hold:

$$\frac{\boldsymbol{f}_{j_2,i_2}^{\mathrm{T}}\boldsymbol{H}_{j_2,k_2}\boldsymbol{p}_{k_2,l_2}}{g_{j_2,i_2,k_2,l_2}\sigma_{\mathrm{s},k_2,l_2}} = \frac{\boldsymbol{f}_{j_2,i_2}^{\mathrm{T}}\boldsymbol{H}_{j_2,k_3}\boldsymbol{p}_{k_3,l_3}}{g_{j_2,i_2,k_3,l_3}\sigma_{\mathrm{s},k_3,l_3}} \tag{61a}$$

$$\vdots$$

$$\frac{\boldsymbol{f}_{j_\tau,i_\tau}^{\mathrm{T}}\boldsymbol{H}_{j_\tau,k_\tau}\boldsymbol{p}_{k_\tau,l_\tau}}{g_{j_\tau,i_\tau,k_\tau,l_\tau}\sigma_{\mathrm{s},k_\tau,l_\tau}} = \frac{\boldsymbol{f}_{j_\tau,i_\tau}^{\mathrm{T}}\boldsymbol{H}_{j_\tau,k_{\tau+1}}\boldsymbol{p}_{k_{\tau+1},l_{\tau+1}}}{g_{j_\tau,i_\tau,k_{\tau+1},l_{\tau+1}}\sigma^2_{\mathrm{s},k_{\tau+1},l_{\tau+1}}} \tag{61b}$$

$$\vdots$$

$$\frac{\boldsymbol{f}_{j_\gamma,i_\gamma}^{\mathrm{T}}\boldsymbol{H}_{j_\gamma,k_\gamma}\boldsymbol{p}_{k_\gamma,l_\gamma}}{g_{j_\gamma,i_\gamma,k_\gamma,l_\gamma}\sigma_{\mathrm{s},k_\gamma,l_\gamma}} = \frac{\boldsymbol{f}_{j_\gamma,i_\gamma}^{\mathrm{T}}\boldsymbol{H}_{j_\gamma,k_1}\boldsymbol{p}_{k_1,l_1}}{g_{j_\gamma,i_\gamma,k_1,l_1}\sigma_{\mathrm{s},k_1,l_1}}. \tag{61c}$$

where each equation corresponds to one square node $\boldsymbol{t}_{j_\tau,i_\tau}$ for $\tau = 2,\cdots,\gamma$. With (14), we see that (60) and (61) respectively reduce to

$$\begin{aligned}&\beta_{j_1,i_1,k_1,l_1} g_{j_1,i_1,k_1,l_1} \sigma_{\mathrm{s},k_1,l_1}\\ &\quad = \beta_{j_1,i_1,k_2,l_2} g_{j_1,i_1,k_2,l_2} \sigma_{\mathrm{s},k_2,l_2},\\ &\beta_{j_\tau,i_\tau,k_\tau,l_\tau} g_{j_\tau,i_\tau,i_\tau,l_\tau} \sigma_{\mathrm{s},k_\tau,l_\tau}\\ &\quad = \beta_{j_\tau,i_\tau,k_{\tau+1},l_{\tau+1}} g_{j_\tau,i_\tau,i_{\tau+1},l_{\tau+1}} \sigma_{\mathrm{s},i_{\tau+1},l_{\tau+1}},\\ &\qquad \text{for } \tau = 2,3,\cdots,\gamma. \end{aligned} \tag{62}$$

Combining the equalities in (62), we further see that (60) holds if and only if

$$\prod_{\tau=1}^{\gamma} \beta_{j_\tau,i_\tau,k_\tau,l_\tau} g_{j_\tau,i_\tau,k_\tau,l_\tau} = \prod_{\tau=1}^{\gamma} \beta_{j_\tau,i_\tau,k_{\tau+1},l_{\tau+1}} g_{j_\tau,i_\tau,k_{\tau+1},l_{\tau+1}}. \tag{63}$$

Thus, Criterion 4 is met if (63) (i.e. (52)) holds for each cycle in $\mathcal{O}$. This concludes the proof.

REFERENCES

[1] "C-RAN: The road towards green RAN, Version 2.5," China Mobile Res. Inst., Beijing, China, White Paper, Oct. 2011.

[2] S.-H. Park, O. Simeone, O. Sahin, and S. Shamai (Shitz), "Joint decompression and decoding for cloud radio access networks," *IEEE Signal Process. Lett.*, vol. 20, no. 5, pp. 503–506, May 2013.

[3] Y. Zhou and W. Yu, "Optimized backhaul compression for uplink cloud radio access network," *IEEE J. Sel. Areas Commun.*, vol. 32, no. 6, pp. 1295–1307, Jun. 2014.

[4] Y. Zhou and W. Yu, "Optimized beamforming and backhaul compression for uplink MIMO cloud radio access networks," in *Proc. IEEE Globecom Workshops (GC Wkshps)*, Austin, TX, USA, Dec. 2014, pp. 1493–1498.

[5] Y. Li and H. Kan, "Complex orthogonal designs with forbidden 2×2 submatrices," *IEEE Trans. Inf. Theory*, vol. 58, no. 7, pp. 4825–4836, Jul. 2012.

[6] V. R. Cadambe and S. A. Jafar, "Interference alignment and degrees of freedom of the K-user interference channel," *IEEE Trans. Inf. Theory*, vol. 54, no. 8, pp. 3425–3441, Aug. 2008.

[7] C. M. Yetis, T. Gou, S. A. Jafar, and A. H. Kayran, "On feasibility of interference alignment in MIMO interference networks," *IEEE Trans. Signal Process.*, vol. 58, no. 9, pp. 4771–4782, Sep. 2010.

[8] G. Bresler, D. Cartwright, and D. Tse, "Feasibility of interference alignment for the MIMO interference channel," *IEEE Trans. Inf. Theory*, vol. 60, no. 9, pp. 5573–5586, Sep. 2014.

[9] I. Santamaria, O. Gonzalez, R. W. Heath, Jr., and S. W. Peters, "Maximum sum-rate interference alignment algorithms for MIMO channels," in *Proc. IEEE GLOBECOM*, Miami, FL, USA, Dec. 2010, pp. 1–6.

[10] M. Razaviyayn, G. Lyubeznik, and Z.-Q. Luo, "On the degrees of freedom achievable through interference alignment in a MIMO interference channel," *IEEE Trans. Signal Process.*, vol. 60, no. 2, pp. 812–821, Feb. 2012.

[11] B. Nazer and M. Gastpar, "Compute-and-forward: Harnessing interference through structured codes," *IEEE Trans. Inf. Theory*, vol. 57, no. 10, pp. 6463–6486, Oct. 2011.

[12] T. Yang, X. Yuan, and Q. T. Sun, "A signal-space aligned network coding approach to distributed MIMO," *IEEE Trans. Signal Process.*, vol. 65, no. 1, pp. 27–40, Jan. 2017.

[13] L. Yang, T. Yang, J. Yuan, and J. An, "Achieving the near-capacity of two-way relay channels with modulation-coded physical-layer network coding," *IEEE Trans. Wireless Commun.*, vol. 14, no. 9, pp. 5225–5239, Sep. 2015.

[14] T. Yang, "Distributed MIMO broadcasting: Reverse compute-and-forward and signal-space alignment," *IEEE Trans. Wireless Commun.*, vol. 16, no. 1, pp. 581–593, Jan. 2017.

[15] H. Cheng, X. Yuan, and Y. Tan, "Compute-compress-and-forward: New results," in *Proc. IEEE GLOBECOM*, Singapore, Dec. 2017, pp. 1–6.

[16] H. Cheng, X. Yuan, and Y. Tan, "Generalized compute-compress-and-forward," *IEEE Trans. Inf. Theory*, vol. 65, no. 1, pp. 462–481, Jan. 2019.

[17] T. M. Cover and J. A. Thomas, *Elements of Information Theory*, 2nd ed. Hoboken, NJ, USA: Wiley, 2006.

[18] D. Slepian and J. K. Wolf, "Noiseless coding of correlated information sources," *IEEE Trans. Inf. Theory*, vol. 19, no. 4, pp. 471–480, Jul. 1973.

[19] U. Erez and R. Zamir, "Achieving 1/2 log (1 + SNR) on the AWGN channel with lattice encoding and decoding," *IEEE Trans. Inf. Theory*, vol. 50, no. 10, pp. 2293–2314, Oct. 2004.

[20] B. Nazer, V. R. Cadambe, V. Ntranos, and G. Caire, "Expanding the compute-and-forward framework: Unequal powers, signal levels, and multiple linear combinations," *IEEE Trans. Inf. Theory*, vol. 62, no. 9, pp. 4879–4909, Sep. 2016.

[21] O. Ordentlich and U. Erez, "A simple proof for the existence of 'good' pairs of nested lattices," *IEEE Trans. Inf. Theory*, vol. 62, no. 8, pp. 4439–4453, Aug. 2016.

[22] R. Storn and K. Price, "Differential evolution–A simple and efficient heuristic for global optimization over continuous spaces," *J. Global Optim.*, vol. 11, no. 4, pp. 341–359, Dec. 1997.

[23] S. L. Loyka, "Channel capacity of MIMO architecture using the exponential correlation matrix," *IEEE Commun. Lett.*, vol. 5, no. 9, pp. 369–371, Sep. 2001.

[24] K. Paton, "An algorithm for finding a fundamental set of cycles of a graph," *Commun. ACM*, vol. 12, no. 9, pp. 514–518, Sep. 1969.

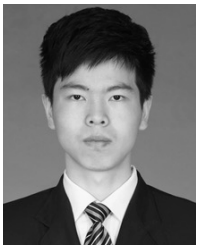

HAI CHENG received the B.Eng. degree from Xidian University, in 2015, and the M.Sc. degree in engineering from the University of Chinese Academy of Sciences, in 2018, where he is supervised by Prof. X. Yuan. His research interests include wireless communication, signal processing, and optimization.

XIAOJUN YUAN (S'04–M'09–SM'15) received the Ph.D. degree in electrical engineering from the City University of Hong Kong, in 2008.

From 2009 to 2011, he was a Research Fellow of the Department of Electronic Engineering, City University of Hong Kong. He was also a Visiting Scholar with the Department of Electrical Engineering, University of Hawaii at Manoa, in spring and summer 2009, and in 2010. From 2011 to 2014, he was a Research Assistant Professor with the Institute of Network Coding, The Chinese University of Hong Kong. From 2014 to 2017, he was an Assistant Professor with the School of Information Science and Technology, ShanghaiTech University. He is currently a Professor with the Center for Intelligent Networking and Communications, University of Electronic Science and Technology of China, supported by the Thousand Youth Talents Plan in China. His research interests include a broad range of signal processing, machine learning, and wireless communications, including but not limited to multi-antenna and cooperative communications, sparse and structured signal recovery, Bayesian approximate inference, and network coding. He has published over 130 peer-reviewed research papers in the leading international journals and conferences in the related areas. He was a co-recipient of the Best Paper Award of the IEEE International Conference on Communications (ICC) 2014, and also a co-recipient of the Best Journal Paper Award of the IEEE Technical Committee on Green Communications and Computing (TCGCC) 2017. He has served on a number of technical programs for international conferences. He is an Editor of the IEEE TRANSACTIONS ON COMMUNICATIONS, since 2017, and also an Editor of the IEEE TRANSACTIONS ON WIRELESS COMMUNICATIONS, since 2018.

TAO YANG (S'07–M'10) received the B.Sc. degree in electronic engineering from the Beijing University of Aeronautics and Astronautics, Beihang University, China, in 2003, and the master's by research and Ph.D. degrees in electrical engineering from the University of New South Wales (UNSW), Sydney, NSW, Australia, in 2006 and 2010, respectively. He was an OCE Postdoctoral Fellow of the ICT Centre, Commonwealth Scientific and Industrial Research Organization (CSIRO), Australia. He was with UNSW as a Research Fellow. He was a Lecturer within the Global Big Data Technologies Centre, School of Computing and Communications, University of Technology Sydney. He is currently with the Beijing University of Aeronautics and Astronautics. He has authored over 60 research articles in the IEEE journals and conferences. His research expertise and interests include physical-layer network coding, multiuser and MIMO, error-control coding, iterative signal processing, and network information theory. He has served as a TPC member of the IEEE ICC and WCNC. He was a recipient of the Australian Postgraduate Award, the NICTA Research Project Award, the Supplementary Engineering Award from UNSW, and the Publication Award from the ICT Centre, CSIRO. He holds an Australian Research Council Discovery Early Career Research Award Fellowship.